

2007-08 WPI SAE Baja Vehicle

A Major Qualifying Project
Submitted to the faculty of
Worcester Polytechnic Institute
in partial fulfillment of the requirements for the
Degree of Bachelor of Science

Submitted By:

Robert Caison

Thomas Dixon

William House

Scott Nelson

Mark Nickerson

Approved:

Kenneth A. Stafford, Advisor

Date: April 26, 2008

Abstract

The objective for this project was to improve upon the 2006-2007 WPI Baja Vehicle for participation in SAE's 2008 Baja Series competitions. Several major vehicle systems were redesigned using both mathematical and computer-aided modeling and simulation. These included the drivetrain, front and rear suspensions, and rear chassis. Improvements in these areas resulted in a lighter and more powerful vehicle that remained as safe and as durable as the previous design. The new parts were fabricated by the team using WPI facilities and with the help of local businesses. The finished vehicle will compete in Illinois (May 08) and Montreal (June 08).

Acknowledgments

We would like to thank:

- AED Motorsports, Indianapolis IN
- Bearing Specialty Company, Worcester MA
- Bodycote Thermal Processing, Worcester MA
- Briggs & Stratton Motorsports
- Ken Jones Tire, Worcester MA
- Polaris, Wyoming, MN
- Vangy Tool Company, Worcester MA
- Ben Mies (WPI)
- Torbjorn S. Bergstrom (WPI)
- John R. Hall (WPI)
- Brendan Powers (WPI)
- Kenneth A. Stafford (WPI project advisor)
- James D. Van de Ven (WPI)

This project would not have been successfully completed without their support.

Table of Contents

ABSTRACT.....	III
ACKNOWLEDGMENTS	IV
TABLE OF CONTENTS.....	V
LIST OF FIGURES.....	VI
LIST OF TABLES.....	VII
1 INTRODUCTION.....	1
2 DRIVETRAIN.....	3
2.1 GOALS.....	3
2.2 ENGINE DYNAMOMETER AND CVT TUNING.....	3
2.3 CVT SELECTION	6
2.4 CHASSIS MODIFICATIONS	7
2.5 SUBFRAME.....	10
2.6 AXLES	13
2.7 CHAIN DRIVE.....	17
3 SUSPENSION.....	22
3.1 OVERALL PERFORMANCE	22
3.1.1 Goals.....	22
3.1.2 Graduate Suspension Analysis	22
3.1.3 Methods.....	24
3.1.4 Results.....	26
3.2 FRONT SUSPENSION	26
3.2.1 Objective	27
3.2.2 Constraints.....	27
3.2.3 Design Envelope.....	28
3.2.3.1 Caster	29
3.2.3.2 Scrub Radius.....	30
3.2.3.3 Ackerman steering.....	31
3.2.3.4 Camber	32
3.2.3.5 Track Width.....	33
3.2.3.6 Toe	34
3.3 REAR SUSPENSION	38
3.3.1 Rear Semi-Trailing Arms	38
3.3.2 Rear Sway Bar Design.....	50
4 IMPACT PROTECTION.....	51
4.1 GOALS.....	51
4.2 MATERIALS SELECTION.....	52
5 CONCLUSIONS & RECOMMENDATIONS.....	55
6 WORKS CITED.....	57
7 APPENDICES	58
7.1 APPENDIX A: SUBFRAME FEA EXAMPLES.....	58
7.2 APPENDIX B: SMALL SPROCKET ASSEMBLY	60
7.3 APPENDIX C: IMPACT MATERIAL DATA	62
7.4 APPENDIX D: MATHCAD SUSPENSION ANALYSIS	64
7.5 APPENDIX E: SPROCKET FEA RESULTS.....	66
7.6 APPENDIX F: ELKA DAMPER SPECIFICATIONS	67

List of Figures

Figure 1: Briggs and Stratton Model 20 Power Graph.....	4
Figure 2: Engine Dynamometer Test Stand.....	5
Figure 3: Brigg's and Stratton Governed Power Curve	6
Figure 4: 2007 Drivetrain Model	8
Figure 5: 2007 Chassis Design	9
Figure 6: 2008 Rear Chassis Design	10
Figure 7: Jigged Subframe Ready for Thermal Processing	11
Figure 8: Complete Rear Drivetrain.....	12
Figure 9: Small Sprocket	18
Figure 10: Large Sprocket Design	19
Figure 11: Experimental Jump Landing Damper Velocities (Terry and Roberts, 2007) ..	23
Figure 12: Baja SAE Tire	29
Figure 13: Caster Angle.....	29
Figure 14: Scrub Radius	30
Figure 15: Ackerman Steering (AutoWare, 1998).....	31
Figure 16: Camber Angle	32
Figure 17: Camber Angle Through Suspension Travel.....	33
Figure 18: Toe In and Toe Out	34
Figure 19: 2007 Final CAD Model	38
Figure 20: 2007 Manufactured Trailing Arm	39
Figure 21: 2007 Rear trailing arm stress distribution landing load case	39
Figure 22: 2007 Rear trailing arm stress distribution 3G cornering load case	40
Figure 23: 2007 manufactured design stress distribution landing load case	41
Figure 24: 2007 manufactured design stress distribution 3G cornering load case	42
Figure 25: 2008 Design in Assembly Model	43
Figure 26: 2008 Design in Assembly Model Landing Load Case	44
Figure 27: Model of 2008 Trailing Arm Design.....	45
Figure 28: 2008 Design 6 Ft. Drop Landing Load Case Stress Plot.....	46
Figure 29: 2008 Design 3G Cornering Load Case Stress Plot	46
Figure 30: The 2nd Major Iteration of the 2008 Trailing Arm Model with FEA Lever ...	47
Figure 31: Last 2008 Design Model with FEA Lever.....	48
Figure 32: Final 2008 Design 3G Cornering Load Stress Distribution.....	49
Figure 33: FEA Results on 2007 Sway Bar	51
Figure 34: Damage to Left and Right Lower Control Arms	52
Figure 35: Factor of Safety Distribution of Stress for Driven Chain Ring	66
Figure 36: Front and Rear Compression Damping	67
Figure 37: Rear Rebound Damping	67
Figure 38: Front Rebound Damping	68

List of Tables

Table 1: Natural Frequency Asymmetry vs. Speed (Tarry and Roberts, 2007)	24
Table 2: Suspension Load Cases Used in FEA.....	40
Table 3: Impact Protection Material Decision Matrix.....	54
Table 4: Damper Linear Regression.....	68

1 Introduction

The SAE Baja Series is an annual series of competitions which originated in 1976. Today, there are three regional competitions in North America and several others around the globe for which university students are tasked to design and fabricate an off-road racing vehicle. These vehicles will compete against approximately 140 other schools in both static and dynamic events. They are supposed to be prototypes which closely represent a product that could be manufactured and sold to the consumer-industrial market. In addition to being durable enough to survive the punishment of rough, off-road terrain, the vehicles must also be manufactured as cheaply as possible because a cost report is submitted along with an engineering design report. Another important objective for every team is to keep the vehicle as light as possible because they must use an unmodified Briggs and Stratton lawnmower engine which produces less than 10 horsepower.

WPI participated in the first Baja competition in 1976, but not again until last year, 2007. The 2007 team (which participated as an MQP for WPI) was very successful, taking home the rookie of the year award and placing highly in the design and endurance events. The project also received first place in the WPI Mechanical Engineering Project Presentation Day.

The SAE Baja vehicle is an excellent MQP because the timely production of a complete vehicle utilizes the engineering and teamwork skills that are emphasized in coursework at WPI and useful in the real world of engineering. The team goes through the entire process of research, design, material and tool sourcing, fabrication, testing, and competition with their vehicle in just one year. The challenges of managing time, budget,

team organization, and relationships with suppliers and any other help are added to the usual difficulties of designing and building a working engineered product.

The 2008 WPI SAE Baja Vehicle was designed to be an improvement upon the 2007 car, with all changes derived from quantitative and qualitative results from the previous summer's competition. The main opportunities for improvement were in the drivetrain and the front and rear suspensions, so these areas were studied and then modified. The new, improved designs for each of these sub-systems are described in detail in this report, in that order.

2 Drivetrain

2.1 Goals

The primary goal of the drivetrain in any performance vehicle is to maximize horsepower delivered to the rear wheels for all practical vehicle speeds. This goal is especially important when attempting to power a recreational off-road buggy with a small, single cylinder engine. All components used in the drivetrain should be durable enough to last through the endurance race, as light as possible, and they should occupy an acceptable space given the restrictions derived from the rest of the vehicle sub-systems, namely the rear suspension. The drivetrain should also contribute to the vehicle's low center of gravity while maintaining 10 inches of ground clearance.

2.2 Engine Dynamometer and CVT Tuning

Based on the results from the 2007 competition in New York, the part of the WPI Baja Vehicle drivetrain that needed the most attention was the Continuously Variable Transmission (CVT). Largely because of the CVT, the team finished poorly in the hill climb and acceleration events and as a result earned an unfavorable starting position (97th out of 140) in the endurance race. In this final event WPI consistently passed other schools in the twisty sections, jumps, and whoops- due to the well-tuned suspension. However, on long straights and uphill inclines they were passed by otherwise slower cars. The CVT was improperly tuned and this error has been corrected in the new design.

A dynamometer plot of the Briggs and Stratton Model 20 Engine can be seen in Figure 1 (Briggs and Stratton, 2008).

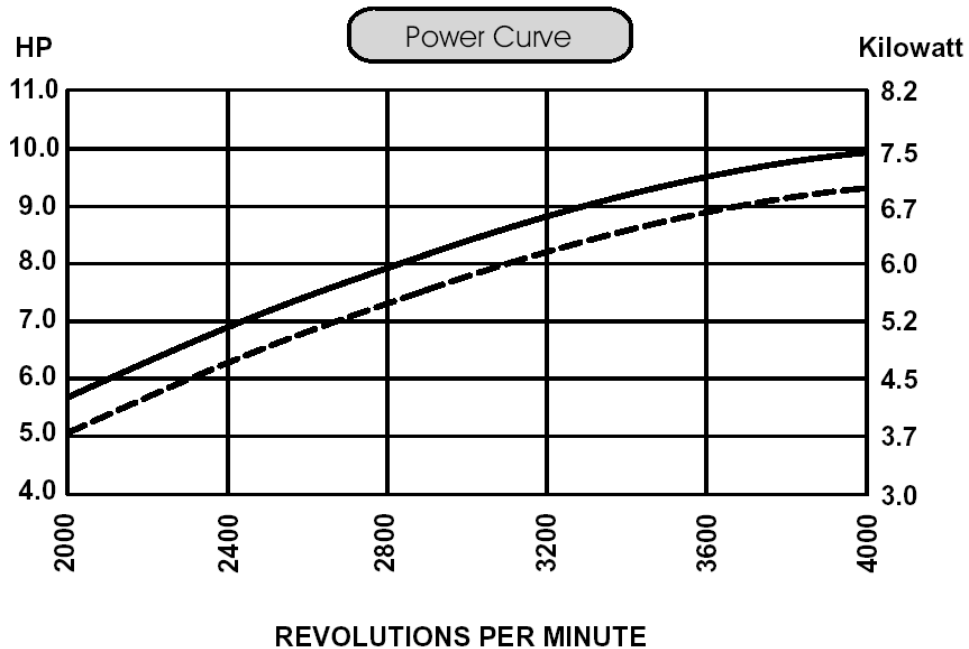


Figure 1: Briggs and Stratton Model 20 Power Graph

Since SAE mandates a 3800 RPM engine speed limit, the CVT was previously tuned to hold the engine at 3700 RPM in order to maximize thrust at the rear wheels. Unfortunately, as the team came to realize, the mechanical governor on the Model 20 is progressive (in contrast to the precise electronic rev-limiters found on most production automobile engines today). The limiter was partially engaging during most of the competition and this severely limited WPI's horsepower.

This year, the first step towards improving the drivetrain was to produce a horsepower curve for the governed engine so that the CVT could be tuned to maintain the proper engine speed. So, in conjunction with two WPI graduate students (Ben Mies and Owen Roberts), the team set up a dynamometer test stand and data acquisition system to measure horsepower and engine speed. See Figure 2 for a picture of this setup. A Stuska water brake and Microstar Laboratories Data Acquisition system was used along with interactive software written in MATLAB. The result of this testing is shown in Figure 3.



Figure 2: Engine Dynamometer Test Stand

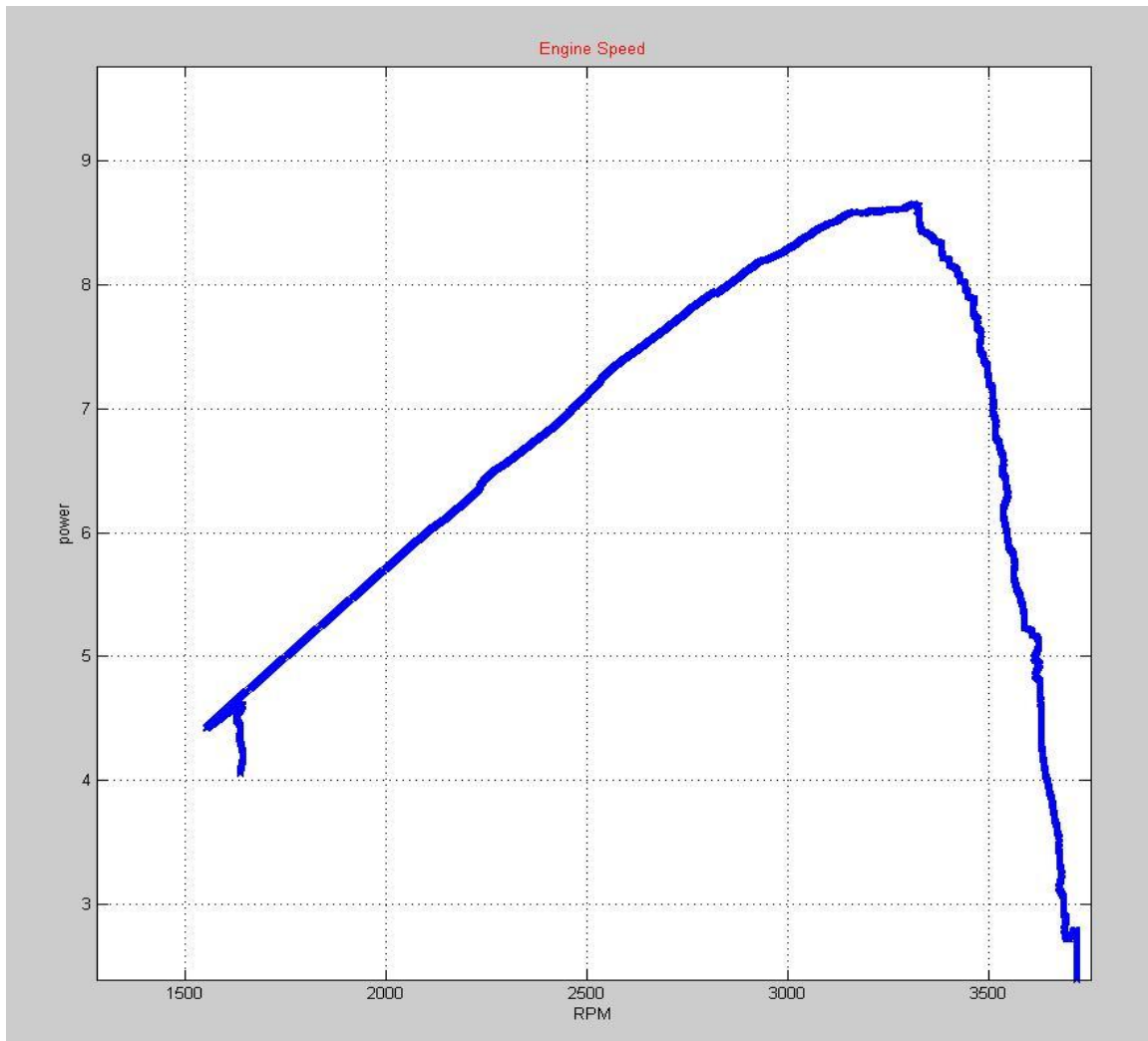


Figure 3: Brigg's and Stratton Governed Power Curve

The CVT should be tuned to 3100-3300 RPM, because after this engine speed the governor drastically reduces power output.

2.3 CVT Selection

In addition to tuning the CVT to hold the engine at the correct rotational speed via internal flyweight, spring rate, and spring preload changes, it is also profitable to choose a properly sized CVT and v-belt as a starting point. In 2007 a Polaris P-90 was chosen due to its proven use in a snowmobiles and convenient interface to the transmission that was being used. Since this transmission has since been eliminated and because the P-90

is optimized for a higher power application than Baja SAE, other options were pursued. Without much analysis, the best choice was decidedly the CVTech Baja Sponsorship CVT which was developed especially for students participating in these competitions. The major problem with other commercially available CVTs in this low-power application is that the sheave side forces of the driven and drive pulleys are both too high, making the CVTech option very attractive. It intentionally produces lower side forces, is easily tuned with the familiar weight and spring changes, is light, and has proven durable by other teams in the past. The dynamometer test stand previously used for engine testing was modified with the addition of a wireless torque transducer and another tachometer to allow for testing of the CVTech CVT and belt. Attempts were made to measure and improve the efficiency of the CVT power transmission, but time constraints limited the useful results to a visual proof that this CVT could in fact be tuned to hold the engine at 3200 RPM. This was a useful result that allowed the rest of the drivetrain to be developed around the CVTech unit with confidence.

2.4 Chassis Modifications

The next easiest area of improvement to the 2007 drivetrain was the elimination of the Polaris ME25P8 two speed (plus reverse) secondary transmission. This unit weighed over 20 lbs without fluid; and during competition only the “high” gear ratio was used. This component was not only heavy and overly complex, but it was also cumbersome in its size, taking up space close to the ground where the engine could otherwise be placed. See Figure 4 for a schematic of the 2007 drivetrain (Forbes *et al.*, 2007), which shows the high center of gravity. A low center of gravity is desired because

during the maneuverability and endurance events, Baja SAE cars have been known to roll over during lateral accelerations.

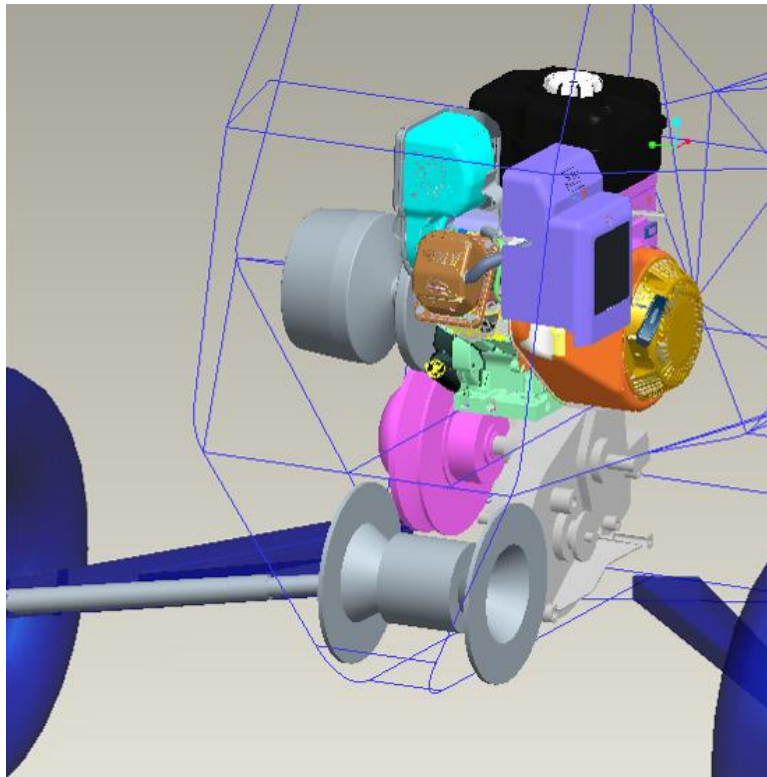


Figure 4: 2007 Drivetrain Model

Mainly through the elimination of the secondary transmission, (but also as a result of several smaller changes), a significant amount of weight and complexity was removed from the back portion of the chassis. As can be seen in Figure 5, the previous structure was not optimized. It contained several cubic sections (tetrahedrons form 3-D trusses to better resolve bending loads into pure tension and compression), and was too large to be protected by the main roll hoop and rear wheels in a rollover or rear end collision.

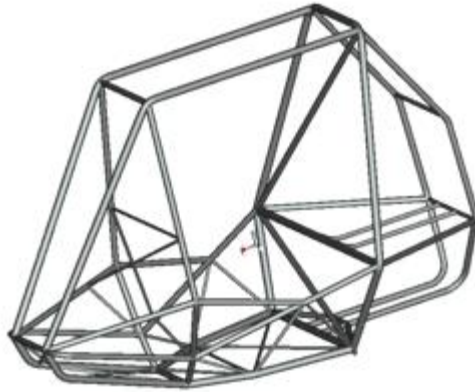


Figure 5: 2007 Chassis Design

This size issue required the use of stronger, heavier tubing, something that is not otherwise required. The only rule about the rear of the chassis is that it must triangulate the main roll hoop, a component already oversized by requirement, so the new chassis tubes and geometry were designed to be compact enough to take advantage of the roll hoop's structural integrity. The new design for the rear of the chassis is shown in Figure 6. It is completely protected in a rollover event and sized to support the weight of the engine, CVT, and subframe, nothing else. All tubes meet at a single node and the rear shock mounts remain braced as a safety precaution. Tubing is .049 inch wall one inch outside diameter normalized 4130 steel. It was welded using ES80-R filler rod and back purged with argon gas. This process maximizes strength without post heat treatment and minimizes the risk of hydrogen embrittlement.

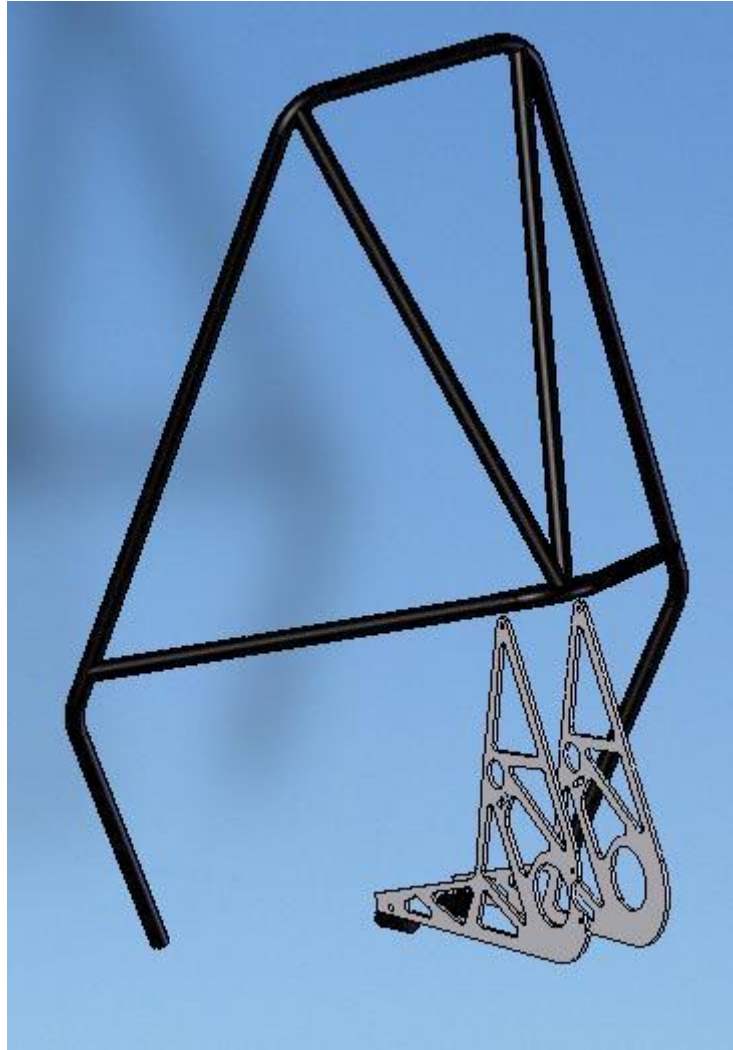


Figure 6: 2008 Rear Chassis Design

2.5 Subframe

As seen in Figure 6, the rear chassis is incomplete without the subframe, shown in grey. This component was manufactured from .260 inch thick 6061 T651 aluminum plate. Aluminum was chosen as a material because of the volume necessary to house four bearings for the chain reduction shafts, which will be discussed in a later section. The shaped aluminum plates were cut by Waterjet; then bearing housings were precision CNC milled to the tightest recommended interference of P6, which is .002 inches (SKF, 2008). The heat treated aluminum was also a good choice because its low density allows

an ideal geometry to be selected for stiffness/weight ratio, which is critical in a housing which supports power transmission shafts. If the shafts and housing combine to deflect more than the bearing oil film thickness, accelerated ball and race wear will occur. All of these conveniences made the aluminum a better choice than the usual 4130 steel tubing, which is thinner in geometry, more challenging to machine, and more dense. 4643 filler rod was used along with the GTAW process to weld in the cross braces (not shown in Figure 6) so that the welds are as strong as the 6061 itself once returned to the T651 condition via heat treatment. Without heat treatment and the use of the proper filler rod, part of the weld heat affected zone could approach the properties of annealed 6061, which has a tensile strength of approximately half that of the T651 (Matweb, 2008). A simple jig was used to position the nine plates that make up the subframe together during the welding and heat treatment process. This jig is shown in Figure 7.

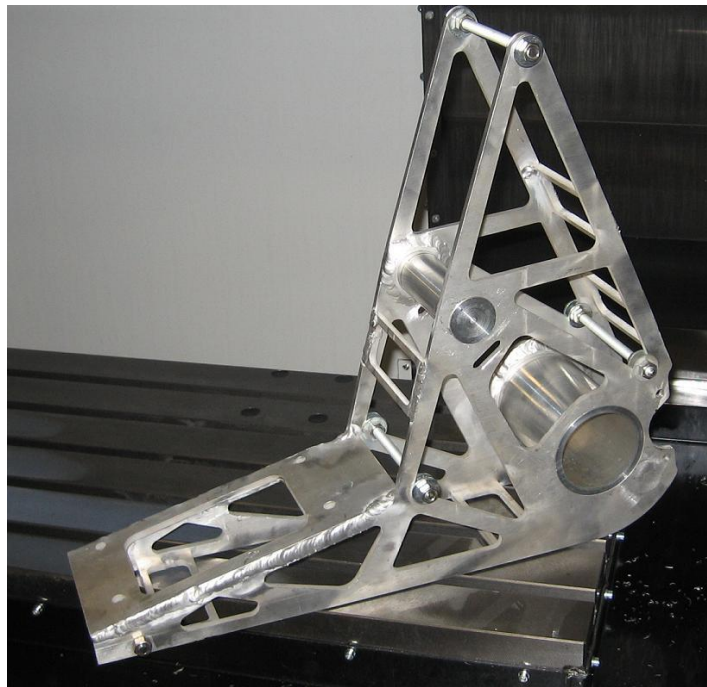


Figure 7: Jigged Subframe Ready for Thermal Processing

To determine the pure geometry of the subframe, extensive CAD work was done in Solidworks. The goals that were kept in mind during each iteration were: keep the engine as low as possible, eliminate as much 4130 as possible in the supporting chassis, avoid interference with the trailing arms during full suspension compression, keep the CVT center distance and side spacing at CVTech’s specifications for our v-belt, keep 10 inches of ground clearance or greater, protect the chain drive setup, ease serviceability, ease the attachment of the rules mandated guards on all rotating components, violate as few chain drive “rules of thumb” as possible, allow a centrally mounted brake caliper, etc. Much iteration was necessary before a satisfactory design was reached, and the result can be seen in Figure 8. Compared to Figure 4, the improvements are evident.

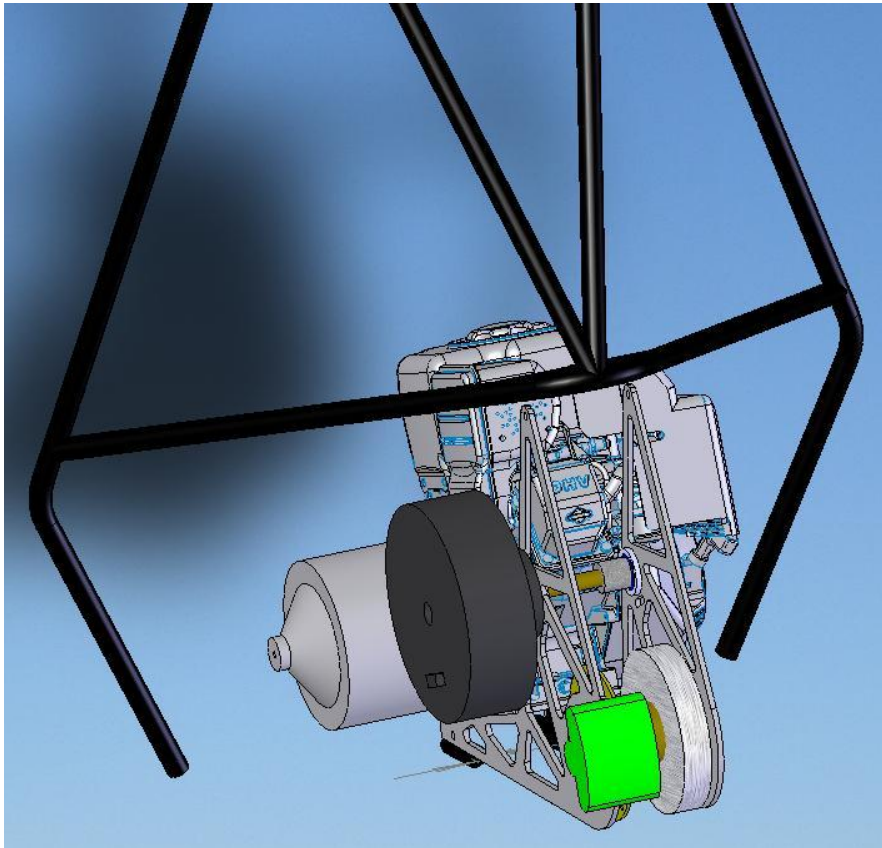


Figure 8: Complete Rear Drivetrain

3 Once the final locations for all drivetrain components the subframe were determined with free body and then optimized using CosmosWorks, the package. The loads that were taken into account skidplating along the length of the bottom side, chain tension, and collision forces produced by the components, especially the 45 lb engine. The number was 30 G, which is the experimentally measured mph frontal collision with an immovable object subframe is designed to support forces generated by it will withstand any reasonable accident and provide use, which is critical given the finite fatigue life of truss cutouts were made in CosmosWorks until the The final result is equally stressed in every beam scenarios. Sample FEA iterations are shown in Appendices

Appendix A: Subframe FEA Examples, with the load case and safety factor indicated.

3.1 Axles

The design constraints on the axles were that they must be 24 inches long to fit the chassis and a maximum of one inch in outside diameter to clear the center section when the rear suspension is in full compression. The axles also had to be made of a material that could be welded to the .83 inch outside diameter splined stubs that fit into the constant velocity joints which worked well in 2007. Several load cases were taken

into account when choosing a wall thickness for the hollow round tube, which was chosen for its high polar moment of inertia to mass ratio and ease of welding to a round stub. Luckily, the wall thicknesses that resulted from most of the load cases provided a favorable inside diameter for welding to the stubs in addition to a reasonable achievable weld thickness and location. Nevertheless, even without consideration of the inherent stress concentration factor at the weld or the fact that the weld metal is probably not as strong as the shaft or stub metal (even post heat-treatment); it will still be the weakest link due to its thinner geometry.

The material chosen for the axles was 4130 steel which will be quenched and tempered to reach a yield strength of 130,000 psi and a shear yield strength of 75,000 psi. This strength number is reached at the highest hardness recommended by Carroll Smith (30 on the Rockwell C Scale) (Smith, 1975), recommended for 4130 without sacrificing endurance limit and impact toughness.

The material needed to be steel for welding to the steel stubs, so the economically available options included mild steel, 4130, or 4340. Mild steel is cheapest but is not strong enough even when using a solid bar of one inch diameter. The 4340 is not commonly available in hollow tube, so the 4130 was a good compromise, especially because it can be easily welded and heat treated.

There are three load cases to consider for the axles. The obvious load case is peak engine torque multiplied through the drivetrain reduction and applied to the axles. This torque is assumed to be transmitted through only one wheel as a worst case scenario, which loads the axle with 520 ft·lbs. This is a load that happens often, so the peak stress in the shaft due to this torsion should be kept well below the failure limit of the material.

The application of this load is generally fully reversed and smooth, with occasional dynamic spikes due to potholes, jumps, etc. For this reason, a fully reversed S-N curve for AISI 4130 was consulted for fatigue data (Norton, 2000). The number of torque reversals per minute is assumed to be 20 over the life of the vehicle. The life of the vehicle is one month of continuous use, which produces the order of 10^4 cycles. At 10^4 cycles, 4130 has decreased to 65% of its original shear strength, or 49,000 psi, and this number will be used to determine wall thickness for this case. The second load case to be considered is impact from rocks, roots, and other course debris. This load is assumed to be glancing as opposed to direct because it would require impractically large axles to prevent plastic bending with a direct impact to the middle of an axle at 40 mph. The drivers of the vehicle will understand that this is a load case to be avoided. The material property in question for a glancing blow is toughness. 4130 at the chosen hardness displays superior toughness (and fracture toughness) than the other steels being considered. The elongation at break is almost 20%, which is outstanding (Matweb, 2008).

The final load case is a landing from a jump on one rear wheel, with the brakes locked up. The force transmitted through the axle is estimated to be 2160 ft-lbs. This assumes 4 G deceleration of the 600 lb car, which determines a normal force that the earth can produce on the tire radius (11 inches) with a maximum coefficient of friction of .9, which is equivalent to a racing tire on asphalt. Luckily, the vehicle should only jump on dirt, where the coefficient of friction is less than half of this number. The vehicle is also unlikely to land with all of its mass on a single rear tire. The drivers will be notified to avoid the brakes during this kind of landing, if possible.

After looking at these load cases, it is clear that assumptions are playing a large role in the final size of the axles. In addition, the largest stress is going to be seen at the weld no matter how thick the axles are, and the weld material is going to be weaker than the rest of the part (ES 80-R has a tensile strength of only 80,000 psi). For this reason the weld itself is going to be more critical than the axles. A thinner axle will actually deform more and transmit less of an impulse through the welds, thereby increasing the life of the assembly. The 4130 steel is also excellent for this reason because high strength steel will deform just as much as mild steel, but will stretch more before plastically failing.

The wall thickness finally chosen for the axles is .095 inch; which produces a convenient inside diameter of .81 inches for welding to the .83 inch stub (will only need to be turned down by .02 inches to fit). This wall thickness produces a maximum stress of 52,000 psi from peak engine torque, which is just above the shear fatigue strength of the material. This is acceptable considering that the engine will not be making peak torque during every one of the 20 load reversals per minute which were assumed, and generally the torque will be split somewhat between the two axles. The load case assumed all the torque was transmitted through one axle.

The load case from a worst case landing will fail the axles. In defense of this situation, the axle stubs can only transmit 295 ft·lbs of torque, and this is not even considering the stress concentration factor of the splined sections where the stubs connect to the constant velocity joints. This means that the new components of the axles are stronger than the already proven pieces which are being reused.

A good compromise has been made with the .096 inch wall 4130 quenched and tempered. It is sufficient for the fatigue of everyday loads, can handle some shock loads,

and is ideal for welding, which is the biggest concern. The axles will not be the weakest link in the drivetrain.

3.2 Chain Drive

As previously discussed, the heavy, two speed transmission was eliminated from the drivetrain. This was made possible by a single chain reduction, which reduces the rotational output speed of the CVT by 6.77 times before the rear axles. The reduction ratio was chosen based on the expected vehicle speeds during operation, which are from 0-40 mph. The 9 tooth small sprocket and 60 tooth large sprocket allow the vehicle to accelerate from 7 to 40 mph while engine speed remains constant at 3200 rpm, the speed of maximum forward thrust force.

Under normal circumstances a sprocket with as few as nine teeth would be avoided, but for the Baja SAE vehicle it was desirable to have the large sprocket as small in diameter as possible for maximum ground clearance. To keep the fixed reduction ratio, it was necessary to use a smaller small sprocket as well, so the nine tooth #35 was chosen. To handle the high chain tension of 4500 lbs under sudden brake application a triple row setup was chosen, which provides a safety factor of just over one in the chain and in the sprocket teeth.

Intelligent design of the small sprocket (see Figure 9: Small Sprocket) and its supporting shaft were crucial, as these components are extremely small and experience high loads. The small sprocket was made from 1040 steel and the small shaft from 4130 steel. The similar carbon content and welding characteristics of the two steels allows them to be welded together and then heat treated to a yield strength of 160,000 psi. The 1040 was chosen for the sprocket because it is more easily machined and does not as

highly stressed as the 4130 shaft, which is severely loaded in bending as opposed to shear and pure compression. The small sprocket was welded to its shaft instead of keyed or splined to minimize stress concentration factors, as the safety factor of the welded assembly is already below two in a worst-case loading scenario. For an assembly view and sample stress analyses of the small sprocket assembly, see Appendix B: Small Sprocket Assembly. The chain tensioning setup is also shown. This system guarantees 180 degrees of chain wrap on the small sprocket for the life of the chain as it wears. Self-lubricating Delrin was used for the chain contact surface, as it has the best wear characteristics and tensile strength of the inexpensive plastics.



Figure 9: Small Sprocket

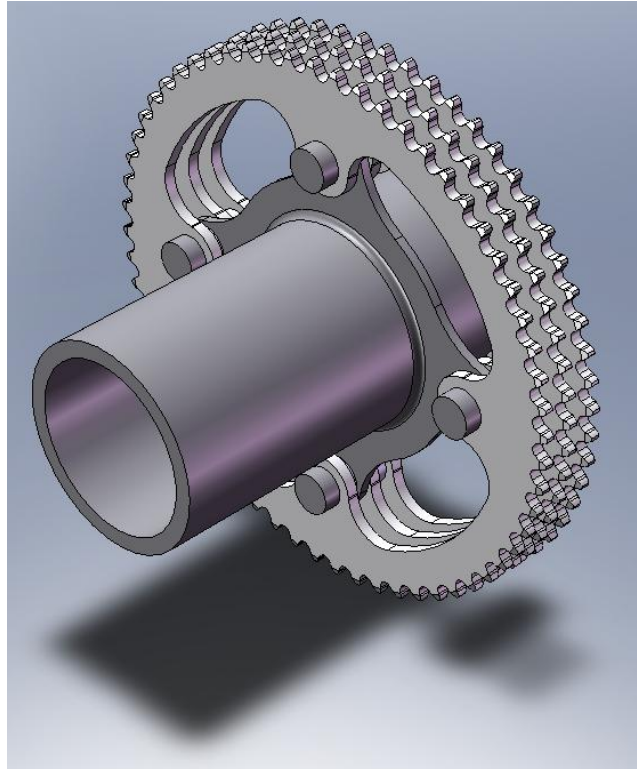


Figure 10: Large Sprocket

In designing the larger of the two sprockets in the chain reduction, four main criteria were considered; strength, weight, manufacturability, and cost. The biggest decision that had to be made with regards to the large sprocket was whether the three chain rings would be manufactured as separate parts, or all together in the same part. It was feasible to fabricate the sprocket from a single large piece of aluminum, however, machining done on the part would be more limited and the part would consequently contain more material and be heavier. Not only that, but the stock material for the part would also cost more as a single large one inch thick block of aluminum would have to be used as opposed to a sheet of $\frac{1}{4}$ inch thick aluminum. Seeing as there was enough 6061 T651 aluminum $\frac{1}{4}$ inch sheet stock left over from the sub frame fabrication to construct the sprocket using the separate chain ring design, it was decided this would certainly be the most cost effective method as new stock would not have to be ordered

saving us several hundred dollars. The initial sprocket design consisted of three 0.16 inch thick chain rings separated with precision spacers to the desired spacing of about 0.234 inches apart. To fix the sprocket to the CV housing, a 1/8 inch thick bracket made from 4130 steel would be used, located flush against one face of the center chain ring. By keeping the bracket as close to the center of the sprocket as possible, bending moments to the bracket tabs (as a result of offset chain forces) were reduced. The chain rings would be fixed to the bracket using four 3/8 inch shoulder bolts, which would also act to align the chain rings. To design the tooth profile of the chain rings, a method outlined by the American Chain Association (American Chain Association, 1982) was used, which took into account a number of factors including the number of teeth and the pitch and spindle diameter of the chain to produce the profile of two teeth. This profile could then be patterned around the chain ring to produce the final chain ring profile. The final design can be seen in Figure 10.

To test the structural integrity of the chain reduction components, an extreme load case had to be simulated. The most extreme load case that could be conceived would be if the wheels came to a complete stop (say after a jump landing), quickly decelerating the inertia of the engine at 6000 rpm/second. It was calculated that the load in the case would put a torque of 1208 ft·lbs on the two axles of the chain reduction. Finite element analysis was run on the final 60 tooth sprocket assembly, which assumed the inside face of the CV housing to be fixed and applied a force to all engaged teeth. With 240 degrees of chain wrap, this meant that 40 teeth on each chain ring were engaged at all times. So, by dividing the force at the teeth ($1208 \text{ ft}\cdot\text{lb} / 0.3075 \text{ ft} = 3928 \text{ lbs}$) by 160 (the total number of engaged teeth), a force of about 32 lbs would be applied to each engaged tooth.

Using this model and a yield strength of 130,000 psi for 4130 steel and 37,000 psi for 6061 T651 aluminum, the factor of safety was plotted and a minimum FOS was found to be 1.4 at the cuff of the tabs on the steel bracket (see Appendix E: Sprocket FEA Results).

Fabrication of the large sprocket was done on a Haas VM-3 3-axis vertical CNC milling machine. SolidWorks was used to model the chain rings and GibbsCAM was used to make the tool paths and produce the G code. The chain rings were produced using three different fixtures. The first fixture consisted of a stock piece of 8.5x8.5x1/4 inch 6061 T651 aluminum strapped to a level piece of scrap stock and the machine table. Four holes were drilled and milled out to a precise diameter of 0.373 +/- 0.001 inches. Two more 9/16 inch holes were drilled out in the center to fixture scrap stock later and the center section of the stock was faced off using a face mill to a thickness of 0.160 +/- 0.005 inches. The next fixture used a scrap piece of level 6061 1/2 inch thick Aluminum, which had six holes drilled and tapped at the same position as the chain ring bolt holes and two featuring holes. The chain ring stock was then bolted to the fixture plate at which point the extra material that was not faced off was faced to the same 0.160 +/- 0.005 inches and the outside of the material was milled down to produce an aluminum disc with a diameter of about 7.5 inches. A 1/4 inch ball endmill was then used to machine a taper along the edge of the disc. The final fixture consisted of the same set up, only the stock was flipped. Now the same taper was added to the other side of the stock using the same ball endmill. Now a 3/16 inch stiff three flute zirconium coated carbide flat endmill was used to mill out the profile of the teeth using a number of small step passes. Finally, a 1/2 inch flat endmill was used to slot out the profile of the inside of the chain ring and the excess material and the finished chain ring were removed. The bracket for the sprocket

was machined in a much similar manner, using the same tapped fixture to hold the stock in place.

4 Suspension

4.1 Overall Performance

4.1.1 Goals

The suspension is one of the most critical components to the Baja SAE vehicle. It is vital that the suspension is responsive enough and has sufficient travel to handle a wide variety of off-road terrain at speeds of 30 to 40 mph. Overall, the goal of the suspension is to keep the vehicle as stable as possible over rough, unpredictable terrain and ensure that all exposed undercarriage members are provided enough clearance to avoid impact with said obstacles.

4.1.2 Graduate Suspension Analysis

Post competition last year, Baja SAE team members Kyle Terry and Owen Roberts conducted a thorough analysis of the Baja SAE vehicle's suspension performance. The goal of this project was to design a more comprehensive computational finite-difference model and run a series of field tests to provide data and recommendations for future suspension optimization.

One of the largest problems they revealed with last year's suspension was an incorrect distribution of the front and rear suspensions natural frequency. This means that the rates at which the front and rear suspension tend to oscillate up and down at (if left unimpeded) were affecting the vehicles performance in a negative way. Using the spring rate, the effective vehicle mass, the damping ratio, and the motion ratio (between wheel and damper travel) one could calculate the natural frequencies of each separate

suspension assembly. It was found that the natural frequencies of the front and rear suspensions were about 2.4 Hz and 2.2 Hz respectively. The goal for natural frequency distribution in an off-road vehicle is to distribute the frequencies such that the rear suspension can “catch up” to the front suspension after an impact with an obstacle at speed.

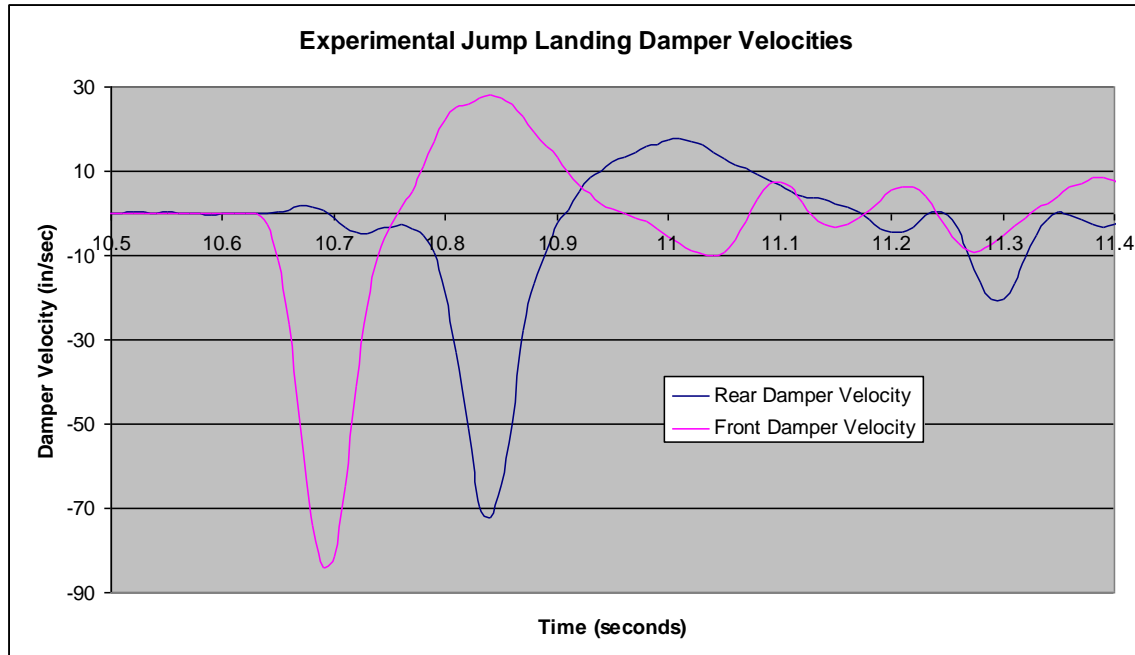


Figure 11: Experimental Jump Landing Damper Velocities (Terry and Roberts, 2007)

This in effect optimizes the vehicles stability over rough terrain and prevents wild front to back oscillations, which can result in slower race time or in more extreme cases, cause the vehicle to flip.

Experimental data collected by Terry and Roberts using potentiometers to measure damper travel over time showed the front and rear damper velocities after an actual jump landing (Figure 11: Experimental Jump Landing Damper Velocities (Terry and Roberts, 2007)). The data, although not very clear due to unpredictable terrain features after the jump, shows how there is an oscillation between the front and back

suspensions and the vehicle does not quickly stabilize itself after the jump. Suggestions by Dixon and Staniforth indicate that the natural frequency distribution for passenger-sized cars at relatively high speeds should be such that the rear suspension's natural frequency is on the order of 10% (Staniforth, 1994) to 20% (Dixon, 1999) higher than the front suspension's. Using their finite difference model, Terry and Roberts were able to calculate suggested natural frequency asymmetries for the Baja SAE vehicle for various speeds from 5 to 50 mph (Table 1). Based on the fact that the Baja SAE vehicle is at top speed (30 – 40 mph) most of the time during competition, it can be interpolated that the natural frequency of the rear suspension should be about 20% higher than that of the front suspension. Last year's suspension had a rear suspension natural frequency that was 15% lower than the front.

Vehicle Ground Speed (mph)	Natural Frequency Increase, Rear Suspension, Relative to Front Suspension
5	136%
10	68%
20	34%
30	22%
50	14%

Table 1: Natural Frequency Asymmetry vs. Speed (Tarry and Roberts, 2007)

4.1.3 Methods

The first problem that had to be overcome in redesigning this year's suspension was the issue of a smaller front A-arm assembly. This year's front suspension design could no longer house last year's front shock assemblies as they were too long. In order to remedy this problem, shorter shocks had to be used. To avoid the cost of purchasing two new shock assemblies (\$2000 - \$3000), the possibility of swapping last year's front and rear shock assemblies was investigated. It was found that with the new front control arms and rear trailing arms, the rear shocks from last year, which were two inches shorter

than the front shocks, could fit in the front, and last year's front shocks could fit in the rear. It was thus decided to go ahead with said design and attempt to optimize the suspension with these constraints.

Once the geometry was more or less fixed, motion ratios between wheel and damper travel were calculated for the front and rear suspension. From here the effective spring rate at the wheels was calculated. Using the suggested spring rates from Terry and Roberts paper of about 375 lb/in for the rear shocks and 250 lb/in for the front shocks and last year's motion ratios, effective spring rates were calculated and then, using this year's motion ratios, the suggested spring rates were translated to fit this year's model (about 290 lb/in in the front and 310 lb/in in the rear). From here one had a good basis to begin analyzing and redesigning the suspension.

To achieve the recommended natural frequencies of about 2.0 Hz in the front and 2.4 Hz in the rear a MathCAD document was created to model the natural frequency of one of the front suspension assemblies and one of the rear suspension assemblies (Appendix D: MathCAD Suspension Analysis). The variables that affected the natural frequency were the sprung mass, the spring rate, the damping coefficient, and the motion ratio. The motion ratios and sprung mass were essentially fixed, thus the variables that could be altered to achieve the desired natural frequencies were spring rate and damping coefficient. Data provided by Elka (the shock manufacturer) on the existing dampers gave the approximate range of damping coefficients from full stiff to full soft for both compression and rebound damping (Appendix F: Elka Damper Specifications). The goal now was to try to achieve spring rates as close to the recommended rates as possible, while keeping within the limitations of the current dampers. This would save having to

send off the dampers to have them rebuilt. It was also decided that since the travel of the front suspension this year would be less, slightly higher spring rates would be desirable to avoid over compression of the shocks and bump-stop contact.

4.1.4 Results

Using the MathCAD model of the front and rear suspension's natural frequencies, final spring rates were selected. It was found that using spring rates of 325 lb/in in the front, 350 lb/in in the rear, full stiff damping in the front, and full soft damping in the rear, natural frequencies of about 2.0 Hz in the front and 2.4 Hz in the rear were achieved. Further modification and analysis of the suspension would now be left to post fabrication testing. Smaller springs used in series could be added and/or modified at this point to play with the spring rate and if damping settings were needed outside the range of the current dampers, different weight oil could be used in the dampers to raise or lower the range of the damping coefficient.

4.2 *Front Suspension*

The front suspension of the vehicle suffered significant impact damage after competition last year. The damage was suffered to the bottom of the lower control arm on one side of the vehicle. It was decided that the best way to alleviate the problem would be to raise the control arms. This could be accomplished by designing and manufacturing our own knuckle. Manufacturing of the knuckle also allowed us to dial in many parameters more precisely than is possible with an off the shelf knuckle designed for an ATV.

4.2.1 Objective

The objective for redesigning the front suspension was to gain more ground clearance while optimizing handling characteristics and reducing scrub. There are many parameters that affect the way an off-road vehicle handles.

4.2.2 Constraints

Using last year's chassis, the design was limited by the pre-existing suspension mounting points. The chassis was heat treated, and welding new tabs or tubes onto the frame would make the heat affected zone and new mounting points weaker than the rest of the chassis. Although it was possible to move them, the current placement was not an issue for design. The wheel base of the car was chosen to remain the same. The wheel base of 64 inches worked well last year for maneuverability and stability. The track width of 61 inches was kept the same as well. SAE Baja rules state that the track width cannot exceed 64 inches, so that the car will be able to fit through all of the obstacles. The team chose 61 inches in the front to provide more space and a buffer zone for tight squeezes. Ride height was also chosen to remain unchanged with ten inches between the chassis and the ground. This decision was due to the fact that the rear suspension geometry was to remain unchanged; keeping the ride height the same would prevent altering the kinematic design of the rear suspension from last year. The previous year designed for 12 inches of travel, and found that it was more than enough. Twelve inches of travel also happens to be the maximum amount that commercially available ball joints can accommodate. The lower control arm length was dictated by the track width constraint along with the width of the chassis at the mounting points. In order to prevent the chassis from hitting the ground at full compression while maintaining the same ride height, the same amount of compression, seven inches, and droop, five inches, were used.

4.2.3 Design Envelope

The suspension design must fit the given constraints while optimizing the most important parameters. Scrubbing of speed in a low power vehicle in a race situation is a major concern. Since the vehicle is already underpowered with limited horsepower, all design parameters that can negatively impact the speed were given top priority.

Ackerman steering, toe, and scrub radius can all potentially cause an increase in scrub between the tire and the ground. Thus, these were some of the first parameters to be set.

The input to the wheels to turn the car is very important in an off-road situation when obstacles are plentiful. Steering control is most affected by caster and toe change. Caster can be easily controlled by adjusting the spacing of the Heim joints that mount the upper control arm to the chassis. This meant that toe change throughout the full range of suspension travel and steering angle became the most important aspect of steering.

Track width is important to the stability and maneuverability of the vehicle. Track width change is a function of the control arm length which was set by track width and chassis width. Track width change was minimized as much as possible. Camber change was not a major concern to the handling characteristics of the car due to round tires. However, if the camber angle became too large, then there tire roll over could occur in a landing situation, adding large moments on the knuckle and control arms. This parameter was also minimized to prevent this possibility. The tire can be seen in Figure 12.



Figure 12: Baja SAE Tire

4.2.3.1 Caster

Caster is the angle of the kingpin (a line drawn between the centers of rotation of the ball joints) in relation to vertical. The caster angle is denoted by X in Figure 13.

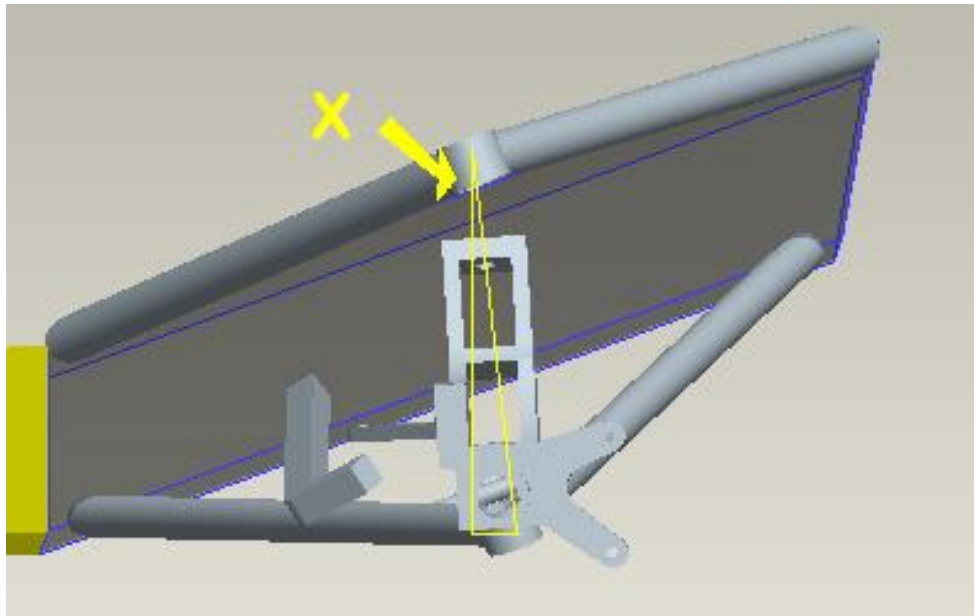


Figure 13: Caster Angle

Caster makes the vehicle steering return to center. When the wheel is turned away from center it lifts the vehicle slightly, therefore the weight of the vehicle will return the wheel to straight. Caster helps make the car more stable by providing resistance, through

the steering wheel, to turning. It also allows less input from the driver on uneven surfaces to keep the vehicle going straight. The downfall of caster is that it requires more input (i.e. force to turn the steering wheel) from the driver to turn the car when compared to a car with 0 degree caster angle.

From testing last years car it was decided that the caster angle was too high. The previous design had a caster angle of eight degrees. The caster this year was designed at 6 degrees. Adjustability was also designed into the system to allow adjustment from 0 to 12 degrees of caster by moving the upper control arms back and forth in their mounts.

4.2.3.2 Scrub Radius

Scrub radius is the distance between the axis of the king pin and the contact patch of the tire on the ground. The scrub radius is denoted by D in Figure 14.

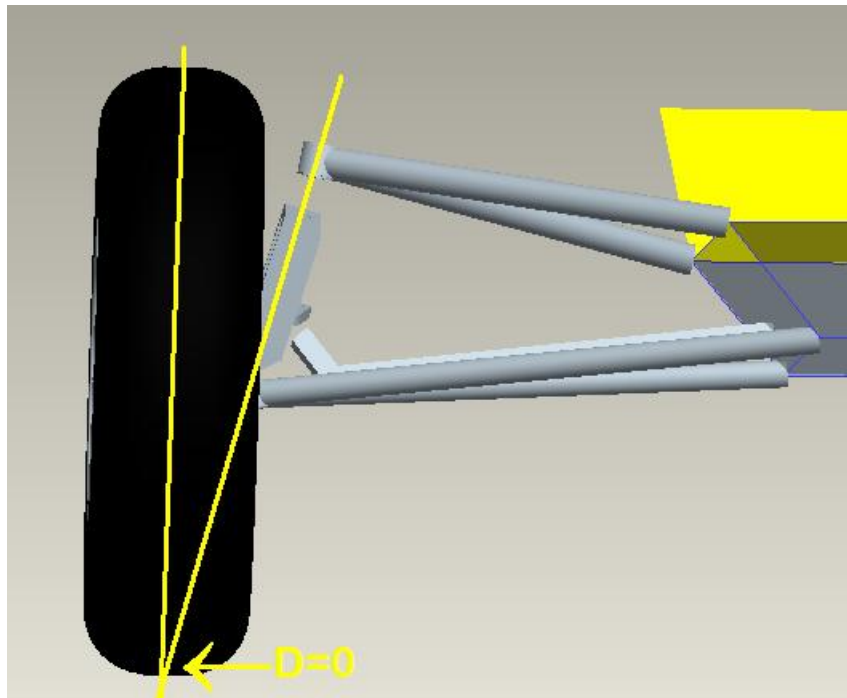


Figure 14: Scrub Radius

The scrub radius was set to zero. A non-zero scrub radius can act as a lever arm trying to turn the wheel. If a significant scrub radius exists in the front and the brakes are applied,

the tire and wheel will attempt to pivot around the king pin axis with only the steering arm to stop it. In an off-road situation when other obstacles could be slowing the wheel down on only one side of the vehicle, it is advantageous to have a scrub radius of zero. The scrub also affects how well the vehicle turns. A scrub radius of zero provides the least friction while turning.

4.2.3.3 Ackerman steering

Ackerman steering is a way to turn the front wheel on the inside of a corner more than the wheel on the outside. If a vehicle is going around in a circle, then the radius of the circle of the outside wheel is greater than that of the inside wheel by the track width, and thus doesn't have to turn as tightly. It is demonstrated in Figure 15.

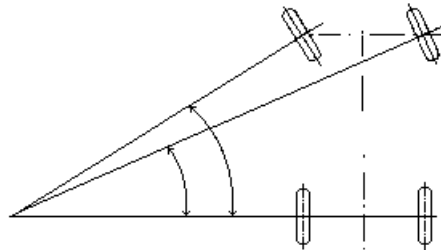


Figure 15: Ackerman Steering (AutoWare, 1998)

Ackerman steering can be accomplished by placing an angle in the steering arm. With the wheels in a straight position, a line is drawn from the king pin axis to the center of the rear axle. If the steering point is placed on that line then 100% Ackerman will be achieved. 100% Ackerman is the configuration that will provide the least amount of scrub, but can also be unstable at high speed shallow turning angles, and encourage over-steer. This would normally be a downfall and is the reason street cars don't run 100% Ackerman. In a vehicle with severely limited horse power it is desired to have as little

scrub as possible, top speed is predicted to be 40 miles per hour, at which it will still be quite stable, and with limited horsepower, over steer is almost impossible.

4.2.3.4 Camber

Camber is the angle of the wheel in relation to the ground. The camber angle is denoted by Y in Figure 16.

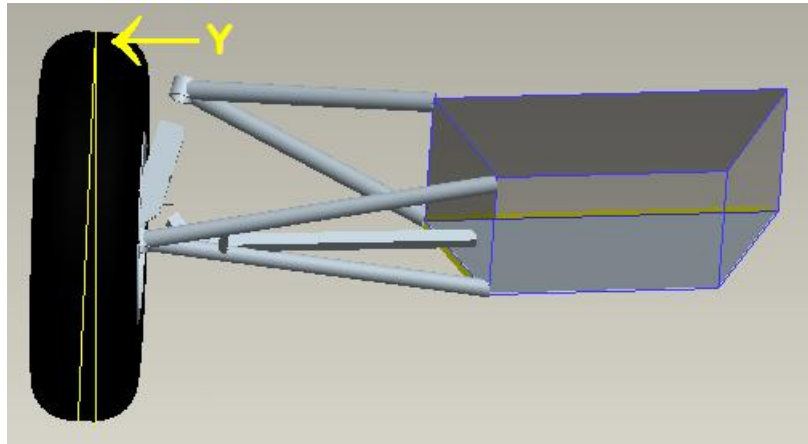


Figure 16: Camber Angle

When the angle Y in Figure 16 is zero and the wheel is perpendicular to the ground, then camber is defined as zero. If the top of the wheel is leaning towards the car then there is negative camber; the opposite yields positive camber. In street cars with semi square tires camber and camber change can have a drastic handling effect. In an off-road situation with rounded tires, the camber will have little if any effect on grip.

The major concern with camber on the Baja vehicle is the possibility of massive stress on suspension components. As the camber angle changes, so does the loading on the knuckle and the control arms. Figure 17 illustrates different angles at different points in a double A-arm suspension. The suspension was designed to minimize camber change as much as possible without disturbing other parameters in the suspension. It was not the most important parameter due to rounded tires.

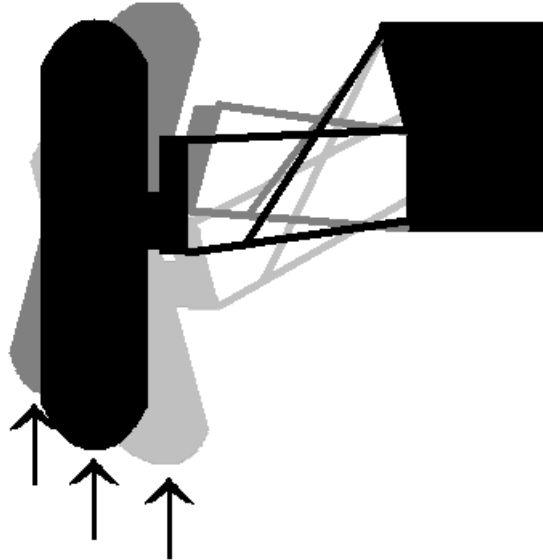


Figure 17: Camber Angle Through Suspension Travel

When the suspension is in compression there is negative camber, placing the upper control arm in compression and the lower in tension. If the suspension is in compression because it is on the outside of the corner then the cornering load will be attempting to place the upper control arm in tension and the lower in compression and canceling some of the load from the normal force of the vehicle.

When the suspension is in droop there is positive camber. This moves the two input forces to the wheel knuckle assembly closer to a vertical line and minimizes the lever arm.

4.2.3.5 Track Width

Track width is the width of the vehicle at the wheels. SAE Baja rules limit the width to 64 inches due to the width of obstacles on the course that the vehicles must fit through. It is not advantageous to be at the full 64 inches because that will not leave any extra space and will cause the driver to slow down to fit the car through. A wide track

width is advantageous for stability issues however. The previous year's vehicle had a track width of 61 inches which is still appropriate.

With a double A-arm suspension, track width change is unavoidable. When the control arms are in line with the frame the track width is at its widest point, any point above or below that will be slightly narrower. The width was set to 61 inches at ride height. The reason being, that if the vehicle was slowed to make a tight maneuver it would maneuver at ride height. Track width change also induces scrub because the wheels must slide to a wider stance and back to a narrower stance without turning. Track width change could not be optimized any farther, because it is a function of control arm length and chassis width which were constraints. The width never exceeds 64 inches and is within the SAE Baja rules.

4.2.3.6 Toe

Toe is the angle of the wheel to the center line of the chassis when trying to go straight. Toe-in is when the front of the tire is towards the inside of the chassis and toe-out is when the front is pointed towards the outside. Toe-in and toe-out are illustrated in Figure 18.



Figure 18: Toe-In and Toe-Out

Without toe-in or toe-out the wheels are pointed straight ahead. This will give the least rolling resistance. Slightly toed-in will provide slight scrub but will give a more

stable ride. When a wheel encounters a disturbance, it is pulled towards the rear around the steering axis. If the vehicle is toed-in this will make the wheel straight and will not initiate a turn. If the vehicle is toed-out, it will turn the wheel more and induce a turn. The car was designed around having slight toe-in.

As stated toe in increase scrubbing, toe-out also increases scrubbing while making the vehicle unstable. Toe change can also steer the vehicle if there is only one wheel on the ground. For these reasons, toe change over the range of the suspension must be minimized.

4.2.4 Design Results

The front suspension utilizes a custom knuckle, with a variation on the previous year's control arm design. The custom knuckle allowed the placement of the ball joint mounting locations in such a way as to optimize all of the given design parameters. The scrub radius was set to zero initially because it achieved the ideal, while still not limiting the design in a significant way. Figure 14 illustrates the actual scrub radius that the knuckle was designed for.

Analysis showed that the 20 degree rake would place the knuckle at a six degree caster based on the control arm geometries, and that adjustment would be very easy. This eliminated the need to iterate the design to optimize caster.

The most important parameter became toe change. This required the knuckle be designed with 100% Ackerman built into the steering arm angle, and then the steering tie rod curve and camber curve had to be matched. When the two curves are not closely matched, as the suspension cycles the wheels are limited by the tie rod length and begin to turn. This condition is known as bump steer and was critical to eliminate in an off-

road course. Through multiple iterations, and raising the steering box one half inch in its mounting plane, a sweet spot was found that placed the vehicle at zero camber at ride height, reduced toe change across the full suspension travel to .45 inches, or 1.3 degrees, and utilized 100% Ackerman.

This kinematic design improved upon the previous year's suspension in multiple areas. The knuckle that was used last year was from a 2006 Polaris Outlaw 500, and actually had negative Ackerman, meaning the inside wheel in a turn would turn less than the outside wheel. Accommodations were made in the steering rack placement but the 100% Ackerman was not possible due to restrictions in rack placement. Toe change was also significantly reduced, from the previous year's 1.4 inches to this year's .45 inches of change. This year's design also reduced the camber angle change and optimized it for dirt. See Appendix G: Front Suspension Design Results for figures detailing the improvements made. Finite element analysis was then iterated to generate the current knuckle and control arm designs.

4.2.5 Manufacturing

The control arms were fabricated from 4130 steel tubing with a .049 inch wall thickness. A 1.25 inch outer diameter was used on the lower control arms while one inch was used on the uppers. With the intention of saving time and materials, the ball joint holders for the upper and lower control arms were saved and reused from 2007. This was also the case with the Heim joint mounts on the upper control arms.

In order to ensure the correct angles and lengths during manufacturing, full size drawings were printed to assist with the layout of the jig. Vices and clamps were laid out

to hold the tubing in the correct locations as printed on the paper. The tubing was notched to fit the cylindrical ball joint holders and then tack welded into place.

After tack welding the tubes in position, the locations of the ball joint holders were double checked. Then the control arms were GTAW welded with inert 4130 filler rod which is designed for 4130 steel that will be heat treated. The control arms will be sent out for heat treatment once completed.

For the upper control arms, a jig was made to hold the Heim joints where they needed to be while the upper control arm was notched to fit. The joint holders were then tack welded, double checked, and welded.

Inside the lower control arm ends there will be PTFE- Filled Delrin bushings. Their housings must be welded with the arms in place on the frame to make sure they are positively in line or the suspension will bind. The bushings were machined out of self lubricating plastic and were pressed into 1.25 OD tubing. The front knuckle will be fixtured, and then the control arm will be notched to fit the suspension mounting points and the knuckle. The shock mount holes will then be fixtured and drilled. The control arms when fully welded will be ready for heat treatment.

The knuckle was machined out of 7000 series aluminum using stock that was already available. Machining was done using six different fixture setups on the HAAS VF-4. The VF-4 was chosen because of its high speed machining capability, and large table. Most material removal was done using a 3 inch face mill at 8000 rpm cutting dry. Incremental depths of .1 inches were used with the face mill, and .125 inches for the few operations that used an endmill. The spindle mounting hole utilizes an interference fit of .005 inches. This is what the Polaris uses and was reasonable given that a steel-steel

press fit is recommended to have .0015 inches of interference, and aluminum is about one third as strong as steel. Ball joint mounting holes were tapered using a ball end mill and a very small incremental depth. Tool path creation was done in ESPIRIT.

4.3 Rear Suspension

4.3.1 Rear Semi-Trailing Arms

The 2007 trailing arms were designed as tube frame structures. The CAD model shown in the figure below was the final model, but the manufactured part differed slightly with the addition of gussets and tube members.

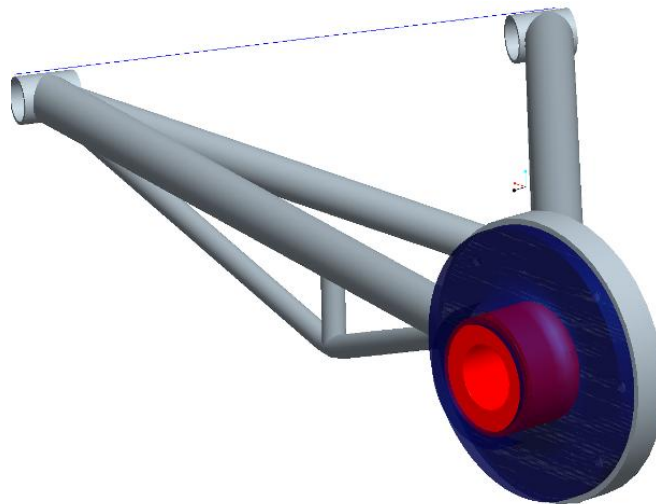


Figure 19: 2007 Final CAD Model

The 2007 design as manufactured is shown below with the gussets and additional tube members. The only parts of the actual trailing arms not included in the model below are the flared holes in the gussets.



Figure 20: 2007 Manufactured Trailing Arm

Finite element analysis was conducted on early design iterations of the trailing arms showing unacceptable deformations and high stresses as shown in the figure below. Analysis was not conducted on the final design as manufactured however.

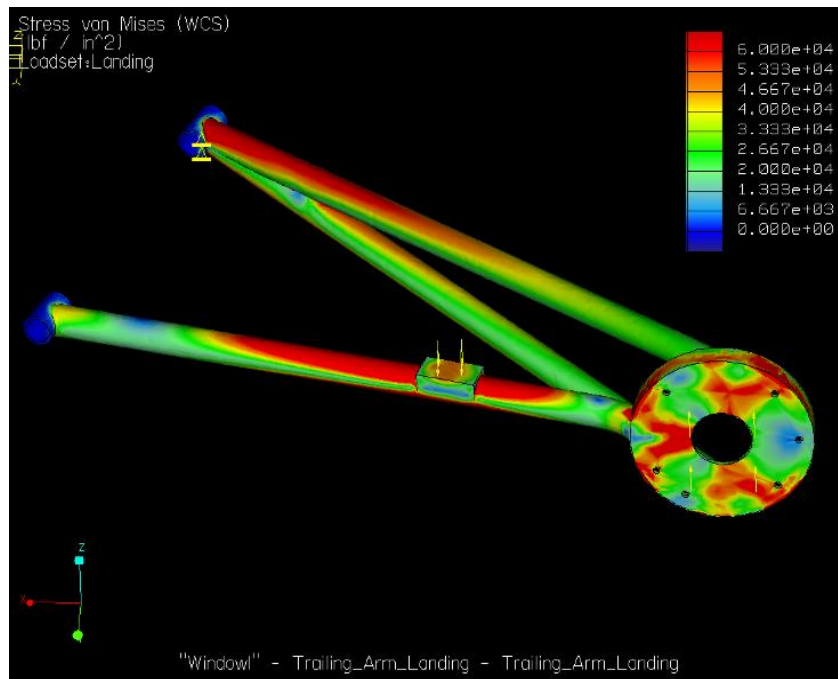


Figure 21: 2007 Rear Trailing Arm Stress Distribution Landing Load Case

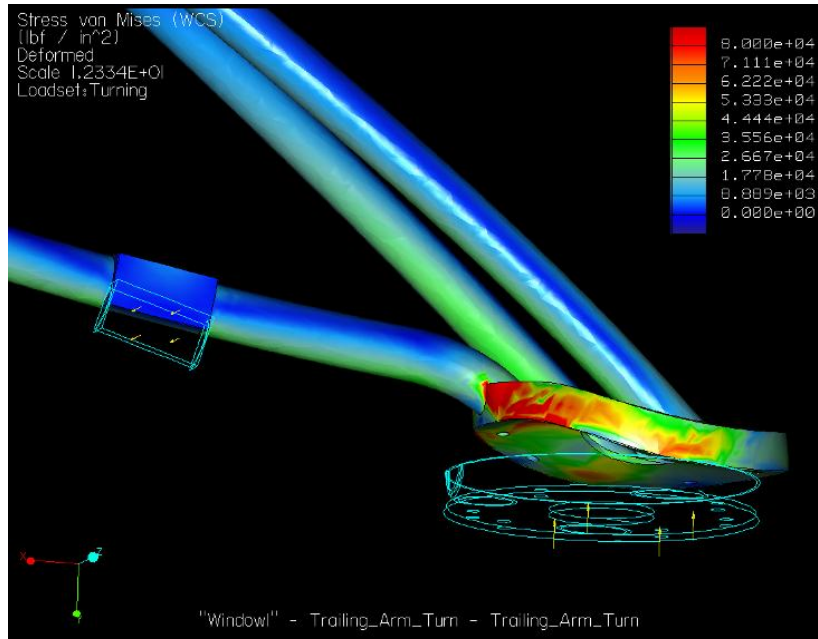


Figure 22: 2007 Rear Trailing Arm Stress Distribution Three G Cornering Load Case

As is shown in the figures above, the stresses in the turning and landing load cases reached 150,000 psi in some areas. These analyses prompted the design modifications reflected in the trailing arm as it was manufactured. The load cases used in these analyses are tabulated as landing and cornering loads in the table below.

Load Case	Bearing Plate Loads (lbf)			Damper Mount Loads (lbf)		
	X	Y	Z	X	Y	Z
Landing	0	0	1500	0	0	-2600
Turning	0	-1800	0	0	0	-350

Table 2: Suspension Load Cases Used in FEA

These load cases were determined by the 2007 team using videos taken of other Baja SAE vehicles landing in competition and estimating vehicle mass and velocity.

These same load cases were also used in the optimization of the 2008 design.

The modifications made to the 2007 design during manufacturing significantly strengthened the trailing arm structure. After the competition, the trailing arms were examined and it was discovered that stress fractures were beginning to form and propagate near the chassis mounts at the heat affected areas of the welds. These cracks,

while only slightly visible, could have easily resulted in catastrophic failure under high cornering or landing loads. It is most likely that these cracks are the result of large, repeated cornering loads at the contact area of the tire causing torsional loads on the structure of the trailing arm. The stiffness of the center area of the structure caused the effect of the torsional load to be concentrated at the chassis mounts. To effectively optimize the 2008 design, FEA studies were conducted on the 2007 design as it was manufactured. The results of these studies are shown in the figures below.

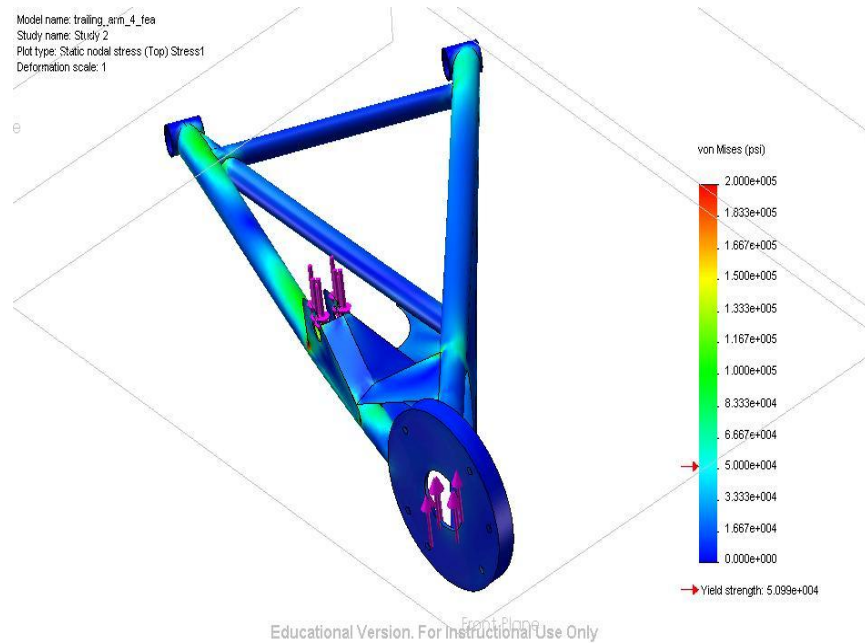


Figure 23: 2007 Manufactured Design Stress Distribution Landing Load Case

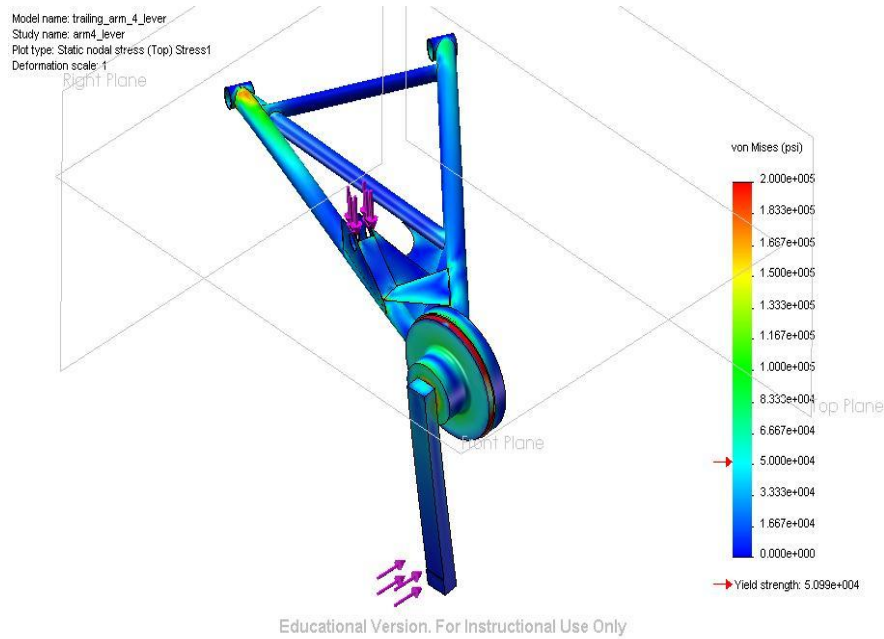


Figure 24: 2007 Manufactured Design Stress Distribution Three G Cornering Load Case

In Figure 24, the protrusion from the spindle face simulates the moment produced by the tire, wheel and spindle assembly. Given the rear tires have a diameter of 22 inches, the aluminum hub was modeled, and the lever was added to the spindle. The lever arm was designed such that it was sufficiently stronger than the rest of the trailing arm that it would not fail or deform before the rest of the model. From these results, it can be clearly seen that the areas of highest stress are seen at the chassis mounts in the cornering load case. It is clear that the 2008 design needed to be significantly stronger while maintaining low weight. In addition, only minimal changes to the geometry of the trailing arm were necessary, as the 2007 kinematic design is quite sound. Slight changes were made to the overall shape of the structure to accommodate shock and damper changes discussed in the shock and damper section.

To increase the torsional strength of the trailing arms, it was theorized that a torque box structure could be utilized. With the addition of a rock crawl event to the competition in 2008, it was also necessary to increase the resistance to point shock loads

from rocks and other debris. Due to the fact that the stress fractures in the 2007 design developed in the heat affected region of the welds at the chassis mounts, it was decided that the 2008 structures would be heat treated to increase the yield strength from approximately 52,000 psi to approximately 130,000 psi for 4130 steel. The first design iteration CAD model is shown in Figure 25. It was modeled as separate plates of .040 inch thick 4130 steel which were then assembled in the Pro/Engineer assembly model. Flared holes were added to the outer plates to increase their bending stiffness. The design of these holes was based on research done by the 2007 team.

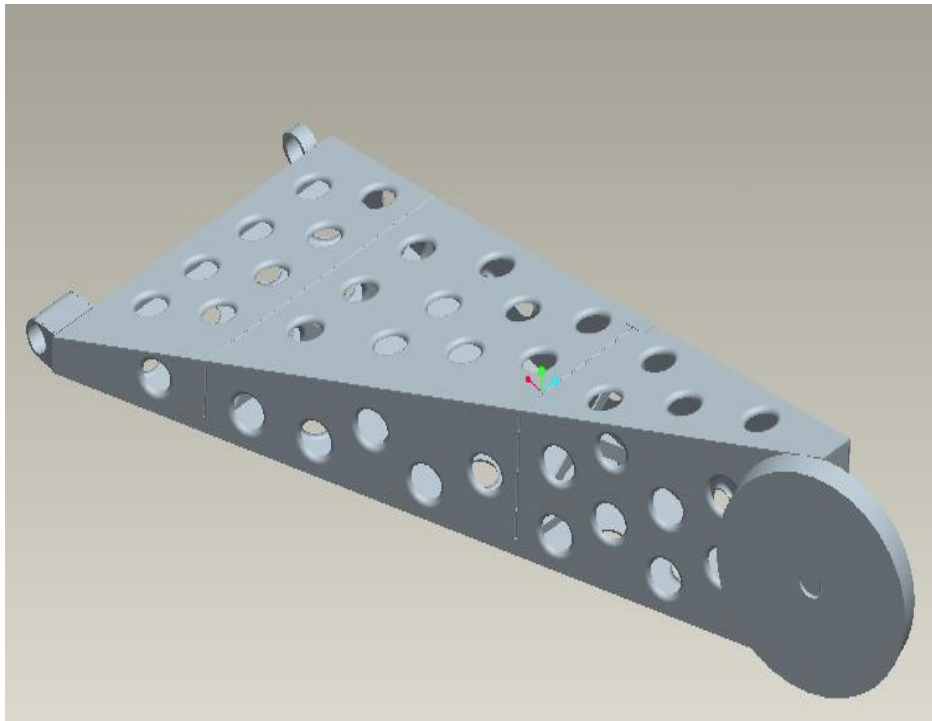


Figure 25: 2008 Design in Assembly Model

This method of modeling the arm made FEA nearly impossible due to the tiny gaps separating each plate at each seam. Meshing and running FEA on the model using the loads tabulated in Table 2 yielded completely erroneous results, as shown in Figure 26.

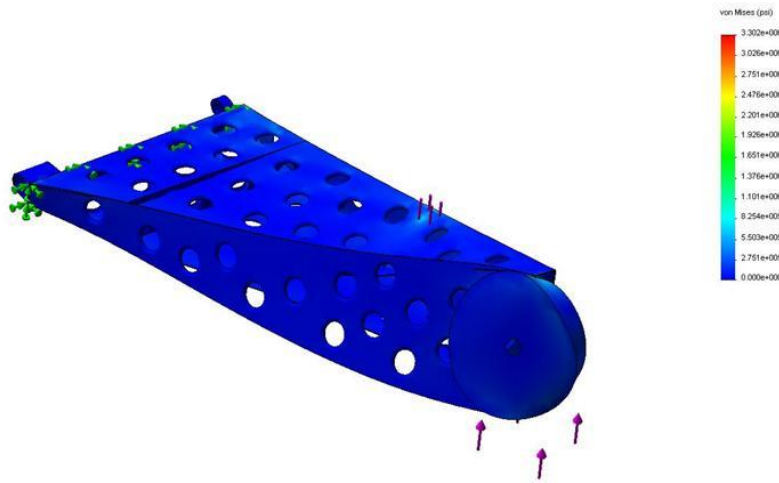


Figure 26: 2008 Design in Assembly Model Landing Load Case

As seen in the figure, the meshing operation failed to connect each plate properly. This is partly due to the surface meshing method used, which relies on the individual surfaces of the model to be selected manually and the thicknesses applied to them. While this method is far more time consuming and complex, it allows for greater control of the mesh. In addition, it was not possible to use “solid” meshing due to the complexity of the model. Also, Pro/Engineer assembly models and constraints do not import properly into SolidWorks where the FEA studies were conducted. Given these results, the trailing arm was completely remodeled as a single solid part using swept blend of two different rectangles at each end. The chassis mount points shown in figure 19 were both changed to Heim joints, and were modeled with more accurate dimensions.

Other modifications to the new model included the addition of cross braces between the two existing braces to strengthen the structure in torsional loading and bending loading. Also, the spindle position was modeled to more accurately reflect its final position at an approximate 15.3 degree angle to the face of the outside (closest to the spindle face) plate. The shock mount was also added to the model, along with

modification of the flared hole placement to eliminate interference with the new cross braces. The results of this redesign are shown in Figure 27.

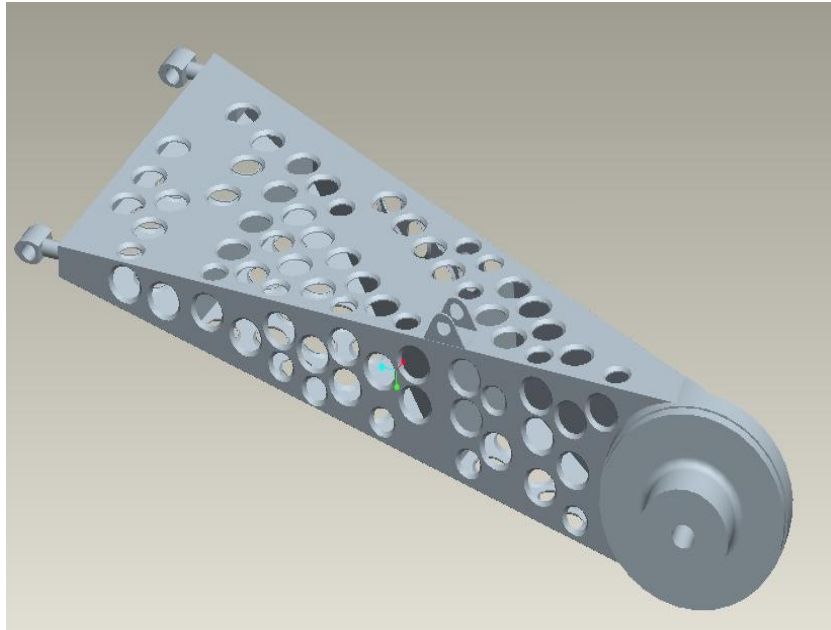


Figure 27: Model of 2008 Trailing Arm Design

Many different analyses were run in SolidWorks to determine placement of the braces and holes. Some of the results are shown in Figure 28 and Figure 29.

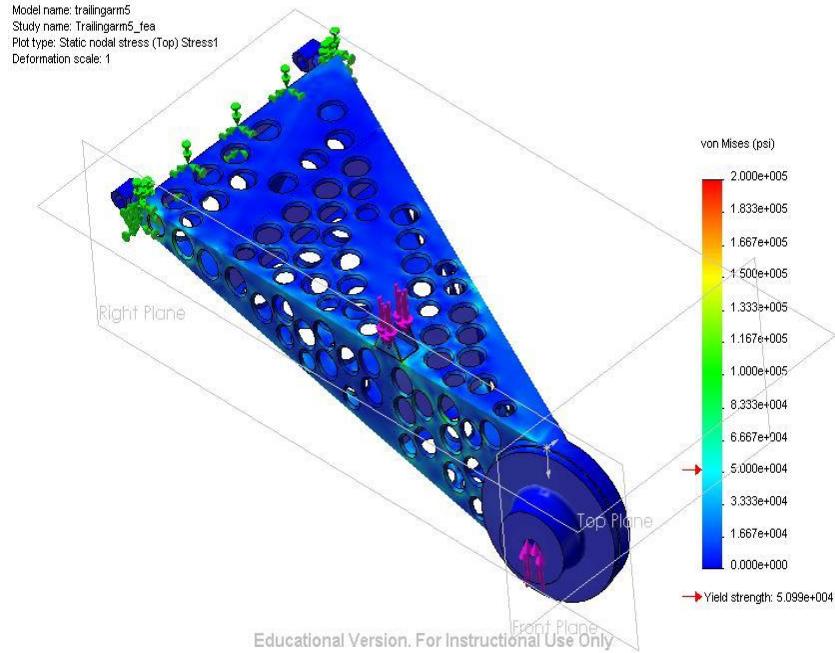


Figure 28: 2008 Design Six Ft. Drop Landing Load Case Stress Plot

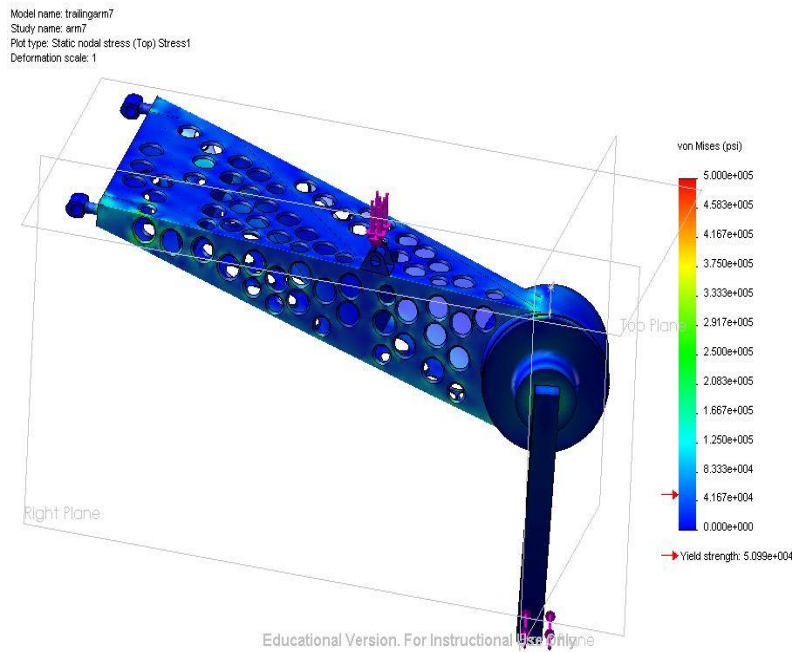


Figure 29: 2008 Design Three G Cornering Load Case Stress Plot

The arm is fixed at the back plate rather than at the chassis mounts because adequate bracing had not yet been added to allow those to be loaded.

Based on these results, the new design was determined to be stronger and suffers from less deformation than the 2007 design. The braces inside the structure however, were shown not to be loaded significantly and seem only to increase the weight and manufacturing complexity.

The trailing arm was again redesigned and re-modeled from scratch to produce a lighter and simpler structure. The end result of this redesign can be seen in Figure 30 below.

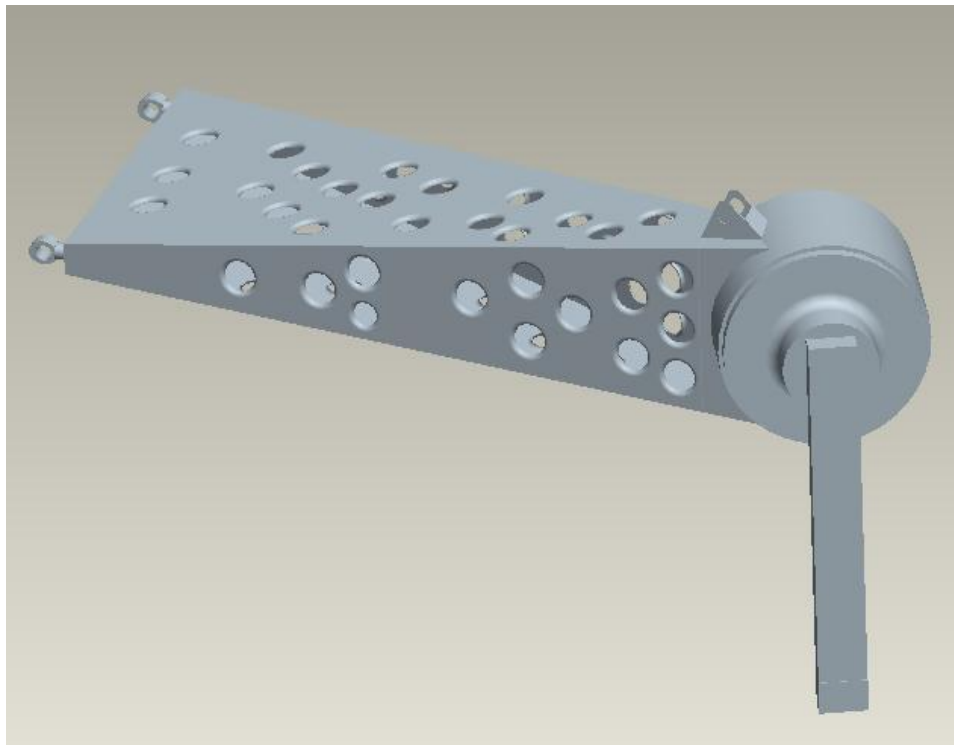


Figure 30: The Second Major Iteration of the 2008 Trailing Arm Model with FEA Lever

This model has new braces and new hole placement to accommodate the change in the mounting points and shock positioning as well as track width changes explained in the shock and damper section. Thickness FEA studies were conducted to determine the optimal thickness of each plate in the model, given the hole geometry. It was determined from those studies that the strength to weight ratio was too high to justify use of .045 inch

or .050 inch thick steel. Due to welding constraints it was determined that use of a thickness less than .040 inches would not provide enough of a weight savings to justify the added difficulty of welding the plates.

The final iteration of the trailing arm used the same braces and mounts as the above model, with the exception of the hole geometry. The placement of the holes was initially optimized to both reduce weight and strengthen the central, unsupported sections of the structure. The final iteration of the trailing arm is shown in Figure 31.

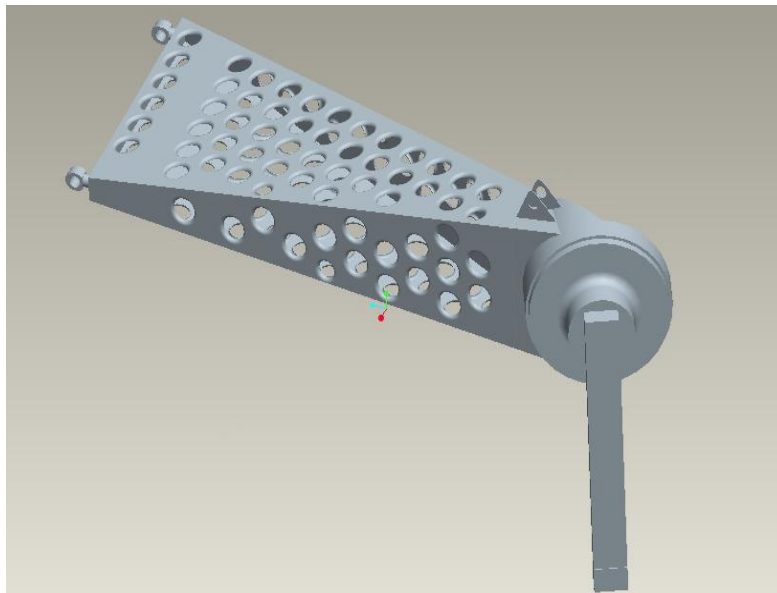


Figure 31: Final 2008 Design Model with FEA Lever

In the above design, the flared holes have been modified to suit the most intense load case, the 3 G cornering load case, and to optimize weight reduction. FEA studies were conducted to determine where stress concentrations would be for the 3 G cornering load case.

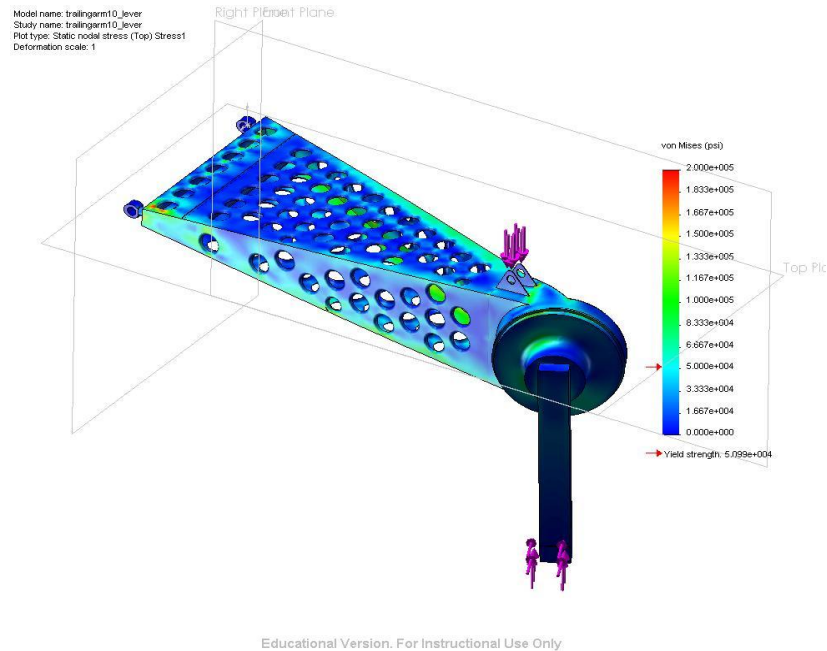


Figure 32: Final 2008 Design 3 G Cornering Load Stress Distribution

These results show acceptable stress distributions throughout the structure. Areas where the stress exceeds 130,000 psi have been modified to eliminate these high stresses. Flared hole placement near the chassis mounts was modified and steel reinforcement blocks were manufactured and placed at the back plate for the Heim joints to be mounted. The blocks were plug welded into the side plates at the rear of the trailing arms increasing the torsional strength in those areas.

Manufacturing the arms involved printing full size drawings of each plate. These drawings were then placed over the .040 inch thick 4130 steel sheet and a center punch was used to mark out each line on the drawings. A scoring tool and straight edge were then used to create the lines of the drawing on the metal. In addition, the center punch was used to mark the center of each flared hole. Once the drawing was successfully transferred on to the sheet metal, the pieces were cut out using a sheet metal shear. This method was chosen to increase the reliability of each cut being straight and to minimize

the material loss compared to what would be seen if the plates were cut with a saw. Each plate was not only sheared along its outer edges but also at the location of each inner brace. This was done to simplify the welding process for attaching the inner braces. Once the plates were all sheared they were ready for the flared holes to be made. This process began by drilling the $\frac{3}{4}$ inch diameter holes. When the holes were drilled, they were flared using the die manufactured by the 2007 team. This process caused significant deformation of each plate. In order to weld the plates together as modeled, they had to be straightened. This was done both by hand and with the assistance of a vice. The edges of the plates were placed in the vice and the plates were then bent slightly to remove the curvature induced by the flaring process. This method worked well to remove the major deformations, but slight deformations and bends in the edges of the plates were still present. These bends did not prove to be a significant difficulty during the welding process. After the plates had been straightened, they were fixtured together individually and tack welded. Full seam welding was delayed until after the spindle canister was fixtured and welded to the rest of the structure. The 6.5 inch diameter spindle canisters were created by shearing a piece of .040 inch thick 4130 steel to a sufficient width to accommodate their full placement on the rest of the structure, and length equal to the circumference of a 6.5 inch diameter circle. The plates were then rolled into canisters of the appropriate shape.

4.3.2 Rear Sway Bar Design

Finite element analysis was conducted on a model of the 2007 trailing arm to determine its stiffness as shown in Figure 33. The results yielded a stiffness of 78 in-lb/deg at the softest setting.

Model name: Part1
Study name: torsionbar
Plot type: Static displacement Displacement1
Deformation scale: 1

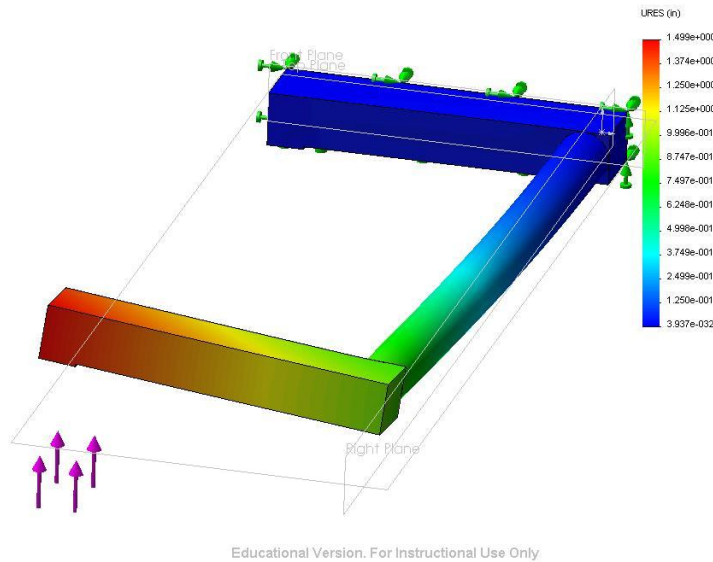


Figure 33: FEA Results on 2007 Sway Bar

From this value, the rear roll stiffness of the 2007 car was calculated to be 1607.13 ft·lbs/deg. Based on recommendations from the 2007 team, the roll stiffness needed to be increased. Maintaining the 2008 rear spring rates and wheel hub deflections, the new desired stiffness of the 2008 sway bar was calculated as 169.143 in·lb/deg. This value doubles the roll stiffness of the car in a cornering scenario where the chassis deflects one degree from vertical. This value also represents the softest sway bar adjustment.

5 Impact Protection

5.1 Goals

During post-competition testing of the Baja SAE vehicle, the forward lower control arms sustained several impacts, which severely dented the forward tubing of both the right and left arms (Figure 34). Such damage could easily have lead to catastrophic

failure of the forward suspension if too great of a force was applied, rendering the vehicle inoperable. If such a failure had occurred in competition, the team would not have been able to advance. As such, it was decided to design impact protection for all members of the vehicle that are prone to impact with rocks and other debris during operation including the forward lower control arms, the rear trailing arms, and the undercarriage of the main frame. The goal here would be to apply a relatively light-weight material to these areas that could absorb and disperse an impact force similar to that which caused the two dents to the lower control arms and prevent any damage to structural components of the vehicle. It would also be ideal if the impact protection could withstand several impacts without being destroyed itself.



Figure 34: Damage to Left and Right Lower Control Arms

5.2 Materials Selection

The first step in the design of impact protection for the Baja SAE vehicle was the selection of an appropriate material. There were many properties cross examined in this

process, but the three main criteria used in the selection of a material were toughness, flexural strength, and density.

Toughness, the criterion that carried the most weight, is a measure of a material's ability to absorb energy. It can be found by looking at the area under the stress-strain plot of a material (the integral Young's Modulus). Since the stress applied to the impact material would most often be a shear stress resulting from a lateral impact, the flexural strength and modulus would be used in the analysis of toughness. Unfortunately, very little data is available on the modulus of toughness of various materials. Alternatively, Izod impact strength is a measure of the amount of energy a material can absorb per unit of thickness (J/cm in most cases) and could be found for a wide variety of polymers and composites. Impact strength is essentially a standardized way of measuring toughness.

A design matrix was created based on these criteria to compare a variety of different materials, which could be used for impact protection. (Table 3) Weighting factors were used to gauge the importance of each criterion and a point value was assigned to each of the four properties of each material. The best material was a polypropylene composite made by Propex Fabrics. This material was very thermoformable, had a low density, and had excellent impact strength. Unfortunately, the material was very expensive and could only be purchased from an overseas distributor and was thus ruled out as an option. Next in line was polycarbonate. Polycarbonate, known by a variety of brand names such as Lexan, has very good impact strength, is relatively light (when compared to other materials on the Baja vehicle), and can be easily thermoformed at temperatures around 300 to 400 degrees Fahrenheit. This material was

much more affordable than the Propex Curv polypropylene composite and was therefore selected for use as impact protection on the SAE Baja vehicle.

		Density	Flexural Strength	Izod Impact Test	Processability	Overall Score
	Weighting Factor (1 - 3)	1	2	3	2	
Property Rating (1 - 5)	Propex Fabrics Curv™ C100A Polypropylene/Polypropylene Thermoformable Composite	5	3	5	5	36
	Polycarbonate	3	4	3	5	30
	Ticona VANDAR® 2100UV High Impact Polyester Alloy	3	3	5	3	30
	Aclo Acculoy POL062L Polycarbonate PET Alloy	3	4	3	4	28
	Kolon KOPA® KN173HI4 High Impact Nylon 6	4	3	3	4	27
	Haysite 54500 Polyester SMC, 35% Glass Reinforced	1	5	3	3	26
	Dow Isoplast® 101 Polyurethane (PUR-RT), Impact Modified	3	3	3	3	24
	Polyvinylchloride	2	3	2	4	22
	ABS	4	3	1	4	21
	High Density Polyethylene	5	1	1	5	20

Table 3: Impact Protection Material Decision Matrix

6 Conclusions & Recommendations

Using a wide range of academic disciplines, the 2008 Baja SAE team was able to redesign the suspension, rear chassis, and drivetrain of the 2007 vehicle to further optimize and improve the previous year's design. The CVT was tuned and optimized such that this year's car will effectively have double the power of last year's. A subframe was designed to reduce weight significantly, lower the center of gravity of the vehicle, increase serviceability, and overall simplify the design. The front suspension was raised to reduce the risk of collisions between the lower control arms and various obstacles and redesigned to optimize toe, camber, and caster and to achieve 100% Ackerman steering. The rear suspension was redesigned to be stronger and more resistant to impact with obstacles and the overall suspension was optimized for better off-road performance. Impact protection was also improved by selecting a stronger and more durable material and by covering more vulnerable members. Overall, the project provided the students with a comprehensive engineering problem that tested nearly every skill learned at WPI. These included mathematical modeling, material analysis, kinematic analysis, solid modeling, finite element analysis, and a wide variety of fabrication techniques.

Due to time constraints testing has not yet been performed on this year's vehicle. As such, it is recommended that future teams run a great deal of testing on the car itself, particularly with regards to suspension performance. Most suspension modifications made to the vehicle were based on purely analytical data. It would be extremely valuable for future teams to collect experimental data with regards to suspension operation in order to fully optimize performance. Due to the outstanding results of last year's model,

it is also recommended that this year's iteration of the model be further improved rather than completely redesigned.

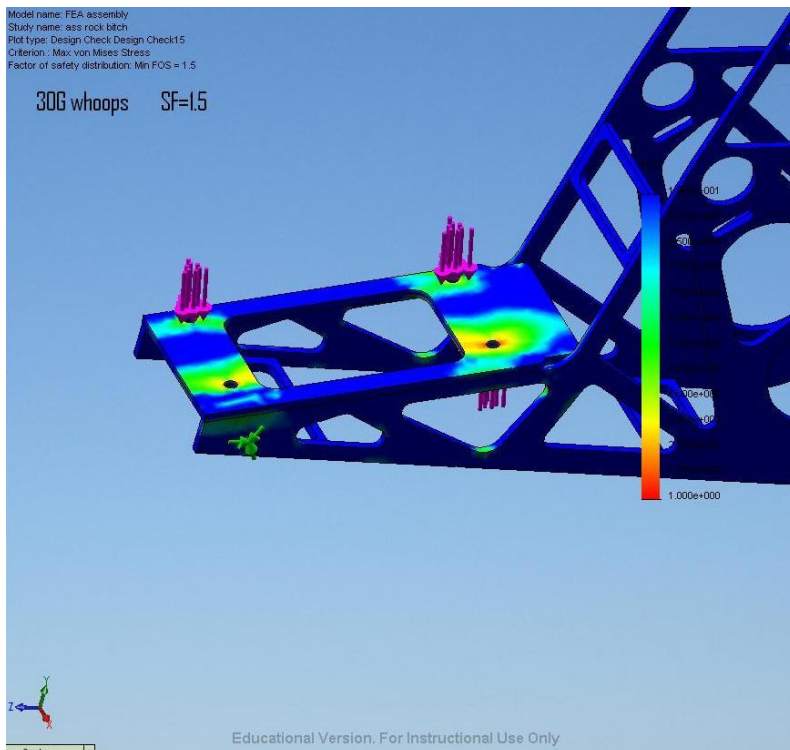
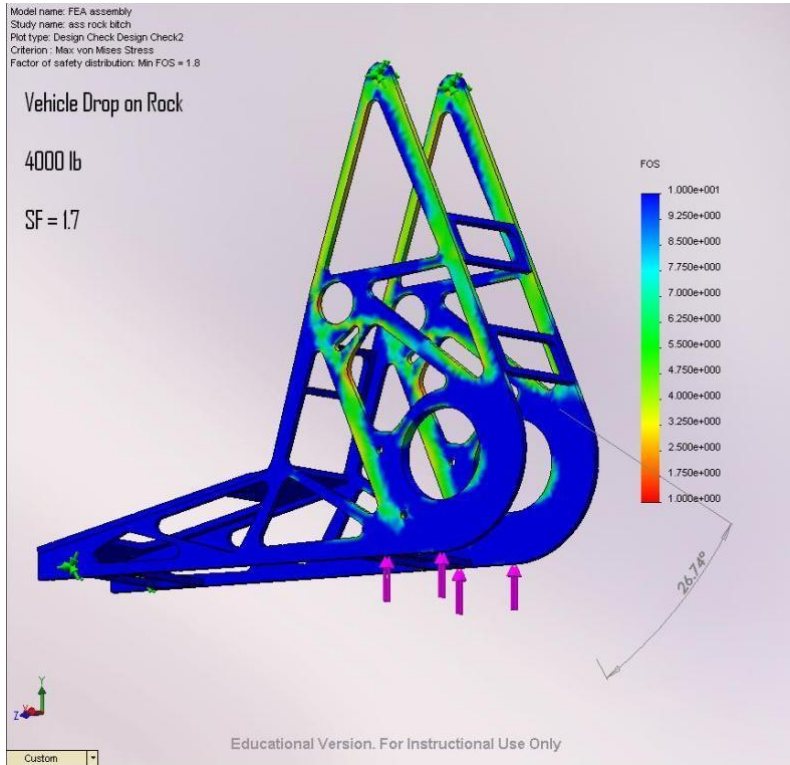
Finally, it is recommended to future teams that internal deadlines be used throughout the project. This year's MQP did not begin until B Term of 2007, when in fact there was enough work to keep a five person team busy from the beginning of the summer or A Term at the latest. Terms B and C were slow because there was no sense of urgency. All the SAE and academic deadlines are not until D Term. In retrospect, it would have been helpful to create artificial deadlines spaced equally throughout the year.

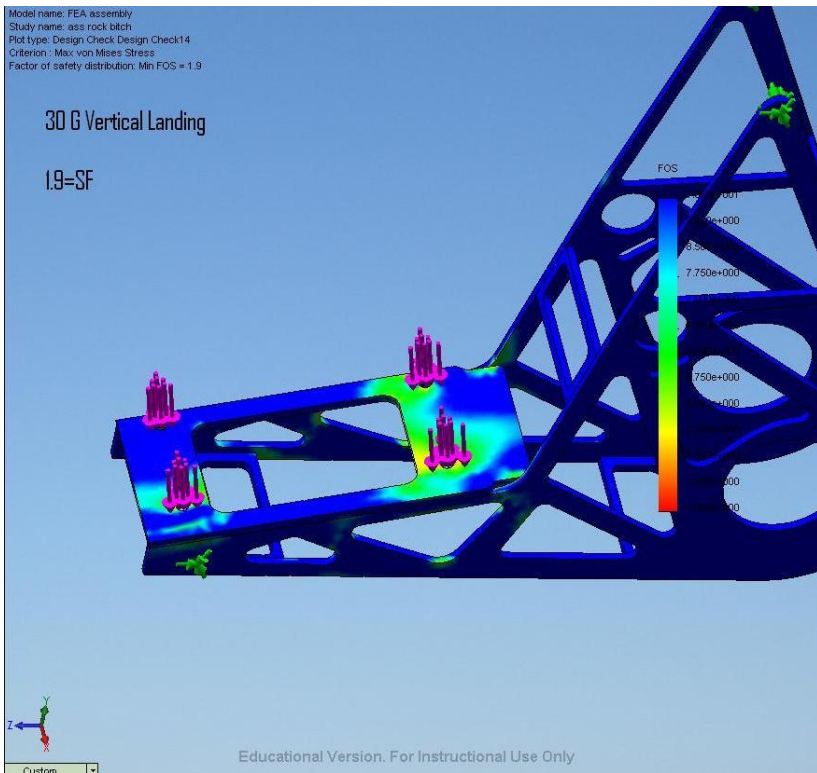
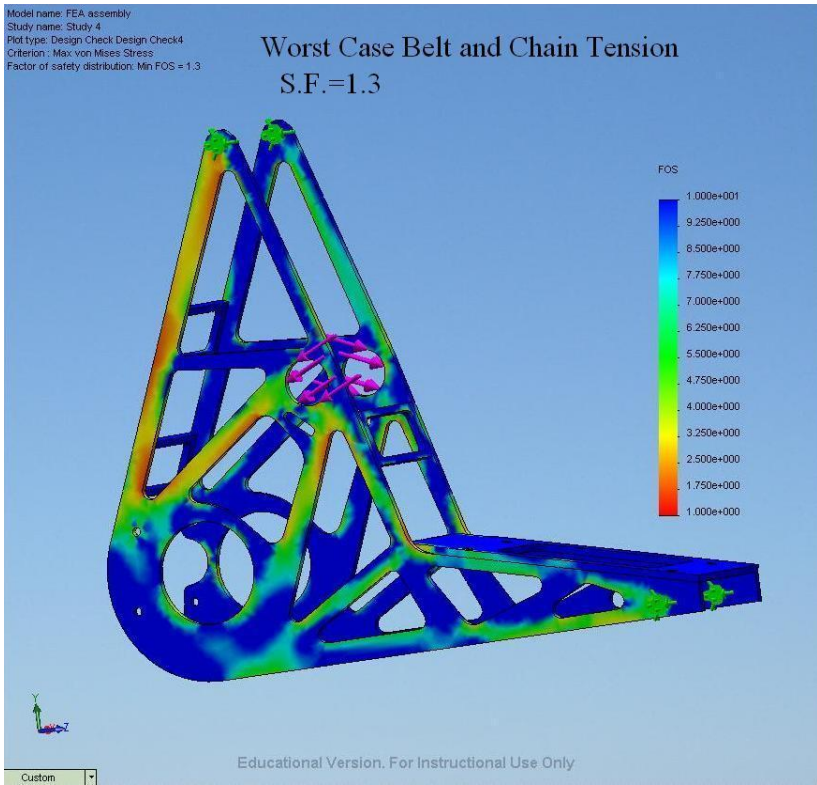
7 Works Cited

- Briggs and Stratton . (n.d.). *Intek OHV 305 Performance Data*. Retrieved 03 16, 2008, from Briggs Racing:
http://www.briggsracing.com/library/Briggs_Racing/pdf/Pages_from_Intek_305.pdf
- Forbes, T., LaPierre, J., Leahy, L., Mies, B., Roberts, J. O., Tarry, K., et al. (2007). *Design and Fabrication of a SAE Baja Vehicle*. Worcester, MA: Worcester Polytechnic Institute.
- Huang, M. (2002). *Vehicle Crash Mechanics*. London, England: CRC Press LLC.
- Matweb. (n.d.). *AISI 4130 Steel*. Retrieved 11 25, 2007, from Matweb- The Online Materials Information Resource:
<http://www.matweb.com/search/DataSheet.aspx?MatID=7500>
- Matweb. (n.d.). *Matweb Search Results*. Retrieved 01 25, 2008, from Matweb- The Online Materials Information Resource:
<http://www.matweb.com/search/QuickText.aspx>
- Norton, R. L. (2000). *Machine Design* . Upper Saddle River, N.J.: Prentice-Hall, INC.
- SKF. (n.d.). *SKF Bearing Reccomended Fits*. Retrieved 02 12, 2008, from SKF:
<http://www.skf.com/skf/productcatalogue/jsp/viewers/tableViewer.jsp?>
- Smith, C. (1975). *Prepare to Win*. Fallbrook, CA: Aero Publishers, INC.
- Dixon, John C. *The Shock Absorber Handbook*. Warrendale, PA: SAE, 1999.
- Staniforth, Allan. *Competition Car Suspension*. Somerset, England: G.T. Foulis & Company, 1994
- Roberts, Owen and Tarry, Kyle. *2007 WPI Baja SAE Dynamic Suspension Analysis*. Worcester Polytechnic Institute, 2007.
- American Chain Association. (1982). *Chains for Power Transmission and Material Handling*. New York, New York. Marcel Dekker, INC.
- AutoWare. (1998). Ackerman Steering and Racing Oval tracks. Retrieved 04 03, 2008 from AutoWare: http://www.auto-ware.com/setup/ack_rac.htm.

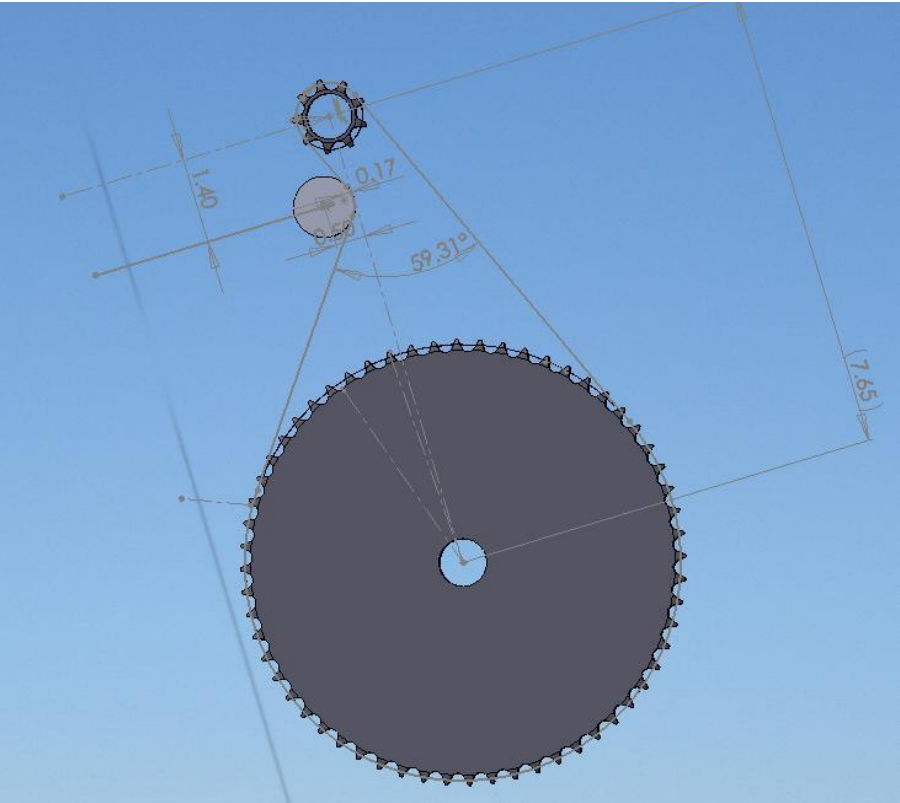
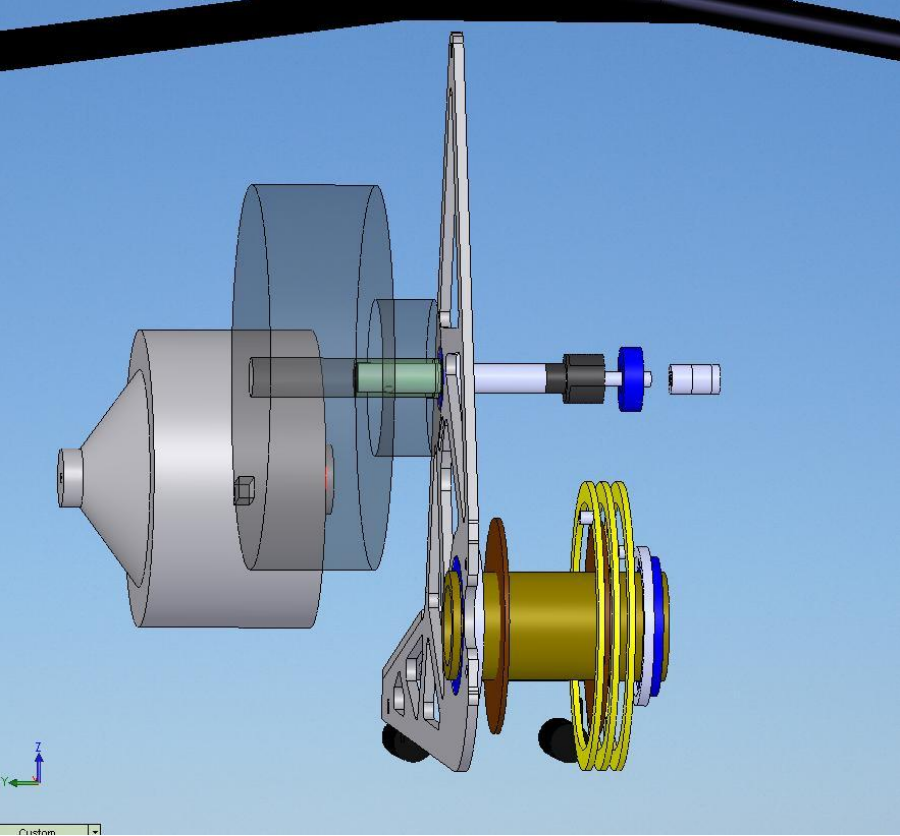
8 Appendices

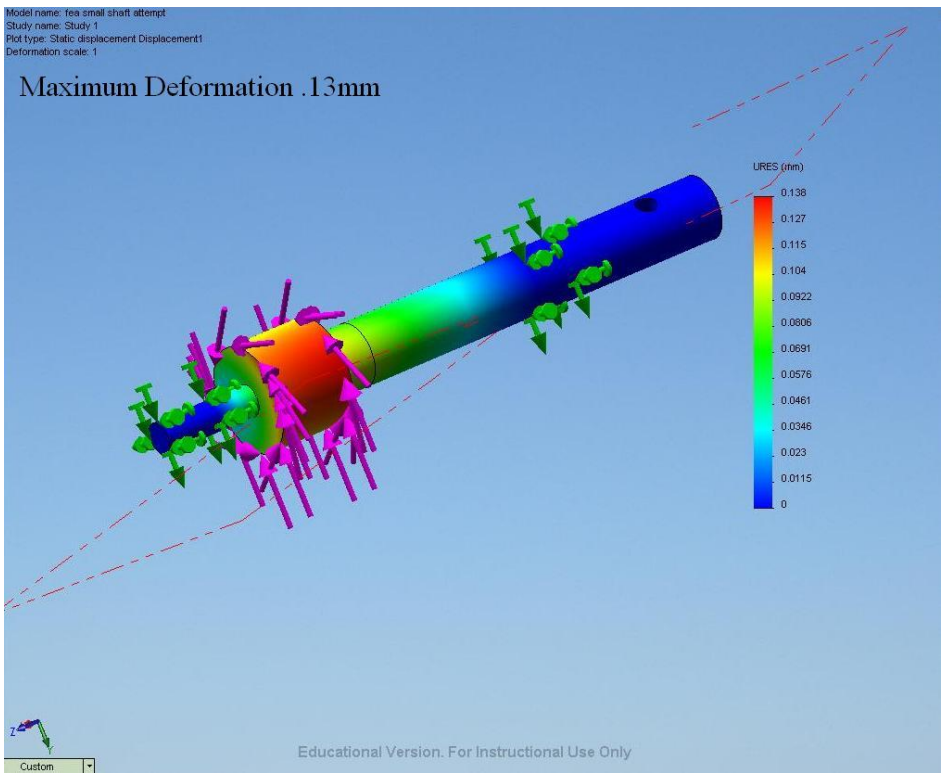
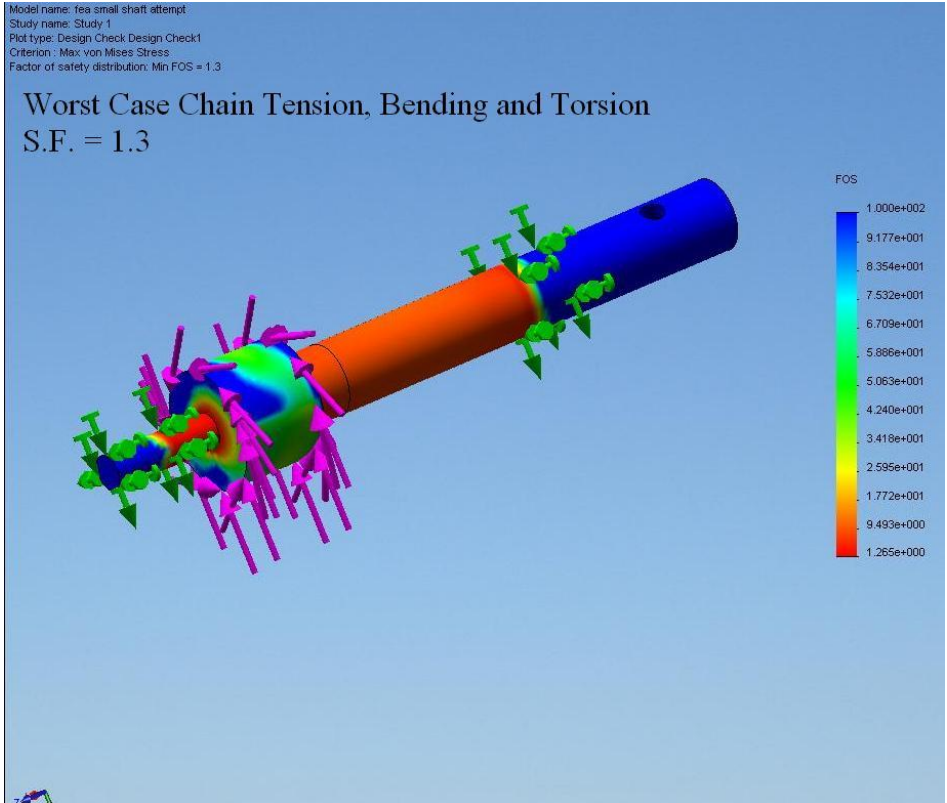
8.1 Appendix A: Subframe FEA Examples





8.2 Appendix B: Small Sprocket Assembly





8.3 Appendix C: Impact Material Data

Category	Material	Flexural Strength (MPa)	Flexural Modulus (GPa)	Density (g/cc)	Izod Impact, Notched (J/cm)	Izod Impact, Un-notched (J/cm)	Charpy Impact, Notched (J/cm)	Charpy Impact, Un-notched (J/cm)	Modulus of Elasticity (GPa)
Polymers	ABS, Impact Grade	75	2.5	1.05	2.89		3.06	11.3	2.06
	Acetal Copolymer	85	2.5	1.41	1.45		0.622	16.3	2.66
	Acrylic	100	3	1.17	0.442		0.303	2.94	2.77
	Nylon 6	85	2.3	1.14	1.86	11.7	1.68	8.98	2.38
	Kolon KOPA® KN173HI4 High Impact Nylon 6	78.5	1.81	1.08	11.8				
	EMS-Grivory Grilon® AZ 3 Unreinforced, High Impact Nylon 66	66	1.8	1.07	10.7				
	Chemlon Polymer Chemlon 280 Nylon 6, High Impact	59	1.6	1.08	9.34				
	Adell AD-10 Nylon 66, Ultra High Impact	72	1.8	1.08	8.5				
	A. Schulman SCHULAMID® 66 MV3HI High Impact Nylon 6/6	71	2	1.07	8.86				
	Polyamide-Imide E-Polymers TEKAMID™ TB120ST , Super Tough PA6, DAM	45	1.4	1.07	9				
	Polyamide-Imide E-Polymers TEKAMID™ TB120ST , Super Tough PA6, DAM	175	5	1.47	0.687	2			6.32
	Polycarbonate	90	2.3	1.2	6.27	12.3	3.34	30	2.37
	Polycarbonate/Acrylic Alloy	78.7	2.22	1.18	7.98	21.4			2.24
	Polycarbonate/PET Polyester Blend	80.3	2.23	1.21	8.08		6.62		1.85
	Aclo Acculoy POL062L Polycarbonate PET Alloy	87	2.5	1.22	12.9				
Polyethylene, HDPE	27.5	1.08	0.954	0.814	2.56	3.15	2.56	1	

	Polyethylene Terephthalate (PET)	133	6.05	1.37	0.787	2.67	0.697	5.91	2.52
	Polyimide	128	8.58	1.31	0.768	7.75			10.9
	Polypropylene A. Schulman PP 1452	40	1.5	0.931	0.782	8.14	1.26	8.05	1.78
	Polypropylene Medium Impact Polypropylene		1.14	0.902	16				
	Polystyrene Dow Isoplast® 101	96.2	3.51	0.908	1.02	4.1	0.885	4.1	3.11
	Polyurethane (PUR-RT), Impact Modified Ticona VANDAR® 2100UV High Impact Polyester Alloy	68	1.8	1.19	12.8		10.5		
	PVC, High Impact	60	1.8	1.23	52.9		7		
	PVC, High Impact	76.6	2.5	1.35	8.56				2.65
Composite	ABS + 30% Glass Fiber	120	7	1.31	0.645	2.61			6.01
	Acetal Copolymer + 30% Glass Fiber Haysite 54500	150	7.5	1.6	1.48	4.81	0.669	3.42	9.01
	Polyester SMC, 35% Glass Reinforced Applied Composites	248		1.7	12.8				
	8068 Polyester SMC	710	34.5	1.83	26.7				
	Propex Fabrics Curv™ C100A Polypropylene/Polypropylene Thermoflexible Composite	80	3.5	0.92	47.5			12	

8.4 Appendix D: MathCAD Suspension Analysis

Rear Suspension

$$K := 350 \frac{\text{lbf}}{\text{in}}$$

Rear Suspension Spring Rate
(largest spring)

$$m := 170 \text{lbm}$$

Effective Mass (rougly 1/4 total mass)

$$Rm := 1.6^2$$

Motion Ratio

$$\omega_0 := \frac{\sqrt{\frac{K}{Rm^2 \cdot m}}}{2 \cdot \pi}$$

$$\omega_0 = 2.753 \frac{1}{s}$$

Undamped Natural Frequency

Compression Damping

$$C_c := 8 \frac{\text{lbf} \cdot \text{s}}{\text{in}}$$

$$\zeta_c := \frac{C_c}{(2 \cdot Rm \cdot \sqrt{K \cdot m})}$$

$$\zeta_c = 0.198$$

Goal Compression Damping Ratio: ~0.2

$$\omega_{dc} := \omega_0 \cdot \sqrt{1 - (\zeta_c)^2}$$

$$\omega_{dc} = 2.699 \frac{1}{s}$$

Rebound Damping

$$C_r := 26.3 \frac{\text{lbf} \cdot \text{s}}{\text{in}}$$

$$\zeta_r := \frac{C_r}{(2 \cdot Rm \cdot \sqrt{K \cdot m})}$$

$$\zeta_r = 0.65$$

Goal Rebound Damping Ratio: ~0.7

$$\omega_{dr} := \omega_0 \cdot \sqrt{1 - (\zeta_r)^2}$$

$$\omega_{dr} = 2.092 \frac{1}{s}$$

Average Damping

$$\omega_{da} := \frac{\omega_{dc} + \omega_{dr}}{2}$$

$$\omega_{da} = 2.395 \frac{1}{s}$$

Goal Average Damped Frequency: ~2.4 Hz

Front Suspension

$$K := 325 \frac{\text{lbf}}{\text{in}}$$

Front Suspension Spring Rate
(largest spring)

$$m := 130 \text{lbm}$$

Effective Mass (roughly 1/4 total mass)

$$R_m := 2.154$$

Motion Ratio

$$\omega_0 := \frac{\sqrt{\frac{K}{R_m^2 \cdot m}}}{2 \cdot \pi}$$

$$\omega_0 = 2.296 \frac{1}{\text{s}}$$

Undamped Natural Frequency

Compression Damping

$$C_c := 11 \frac{\text{lbf} \cdot \text{s}}{\text{in}}$$

$$\zeta_c := \frac{C_c}{(2 R_m \sqrt{K \cdot m})}$$

$$\zeta_c = 0.244$$

Goal Compression Damping Ratio: ~0.2

$$\omega_{dc} := \omega_0 \cdot \sqrt{1 - (\zeta_c)^2}$$

$$\omega_{dc} = 2.226 \frac{1}{\text{s}}$$

Rebound Damping

$$C_r := 25.4 \frac{\text{lbf} \cdot \text{s}}{\text{in}}$$

$$\zeta_r := \frac{C_r}{(2 \cdot R_m \sqrt{K \cdot m})}$$

$$\zeta_r = 0.564$$

Goal Rebound Damping Ratio: ~0.7

$$\omega_{dr} := \omega_0 \cdot \sqrt{1 - (\zeta_r)^2}$$

$$\omega_{dr} = 1.896 \frac{1}{\text{s}}$$

Average Damping

$$\omega_{da} := \frac{\omega_{dc} + \omega_{dr}}{2}$$

$$\omega_{da} = 2.061 \frac{1}{\text{s}}$$

Goal Average Damped Frequency: ~2.0 Hz

8.5 Appendix E: Sprocket FEA Results

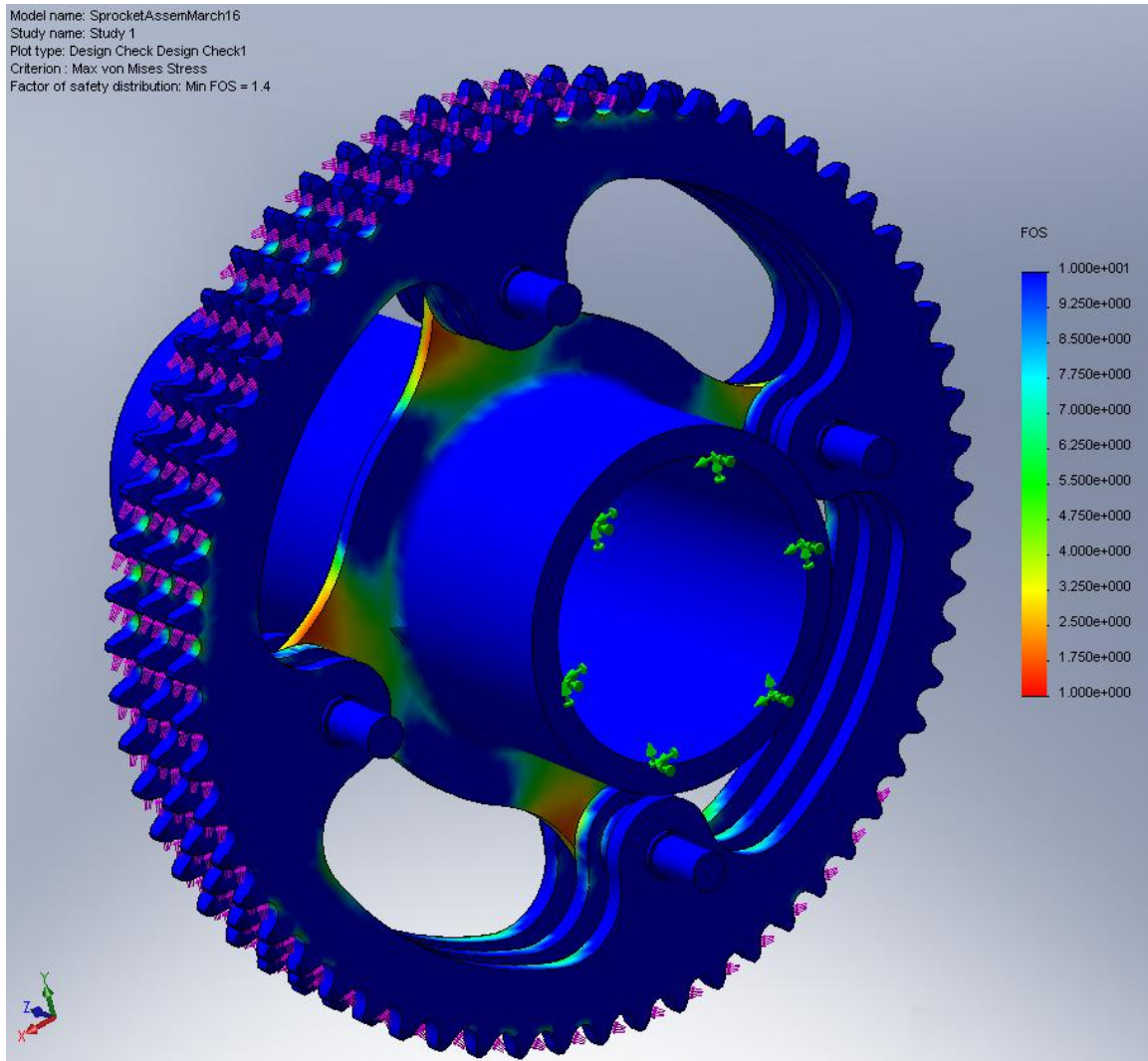


Figure 35: Factor of Safety Distribution of Stress for Driven Chain Ring

8.6 Appendix F: Elka Damper Specifications

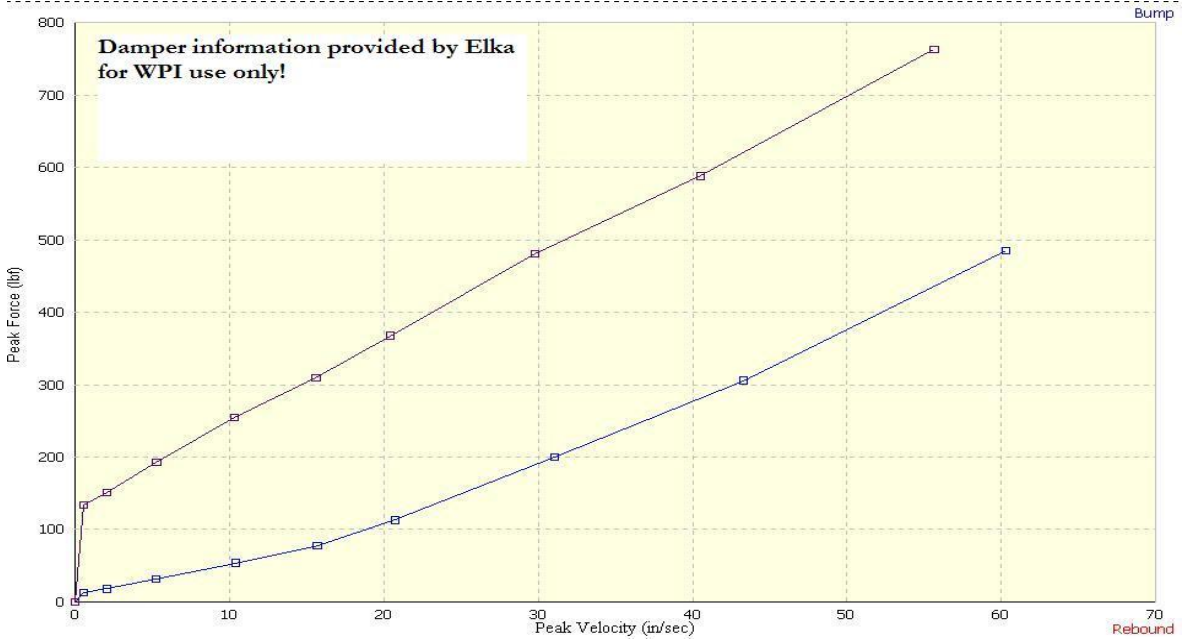


Figure 36: Front and Rear Compression Damping

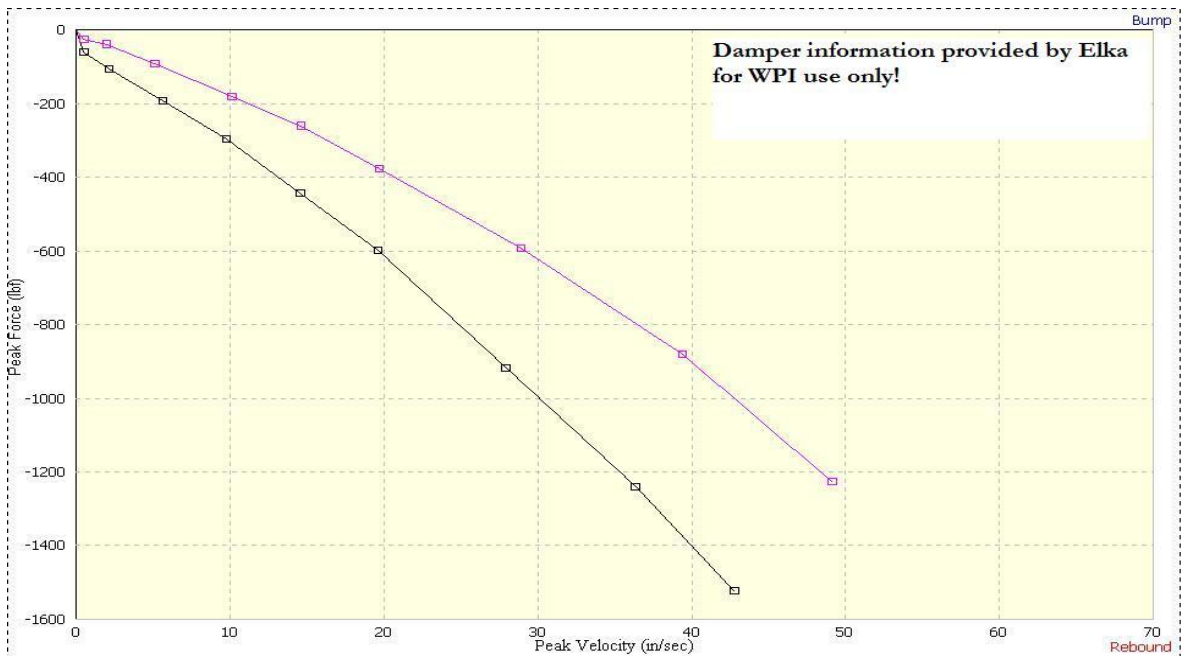


Figure 37: Rear Rebound Damping

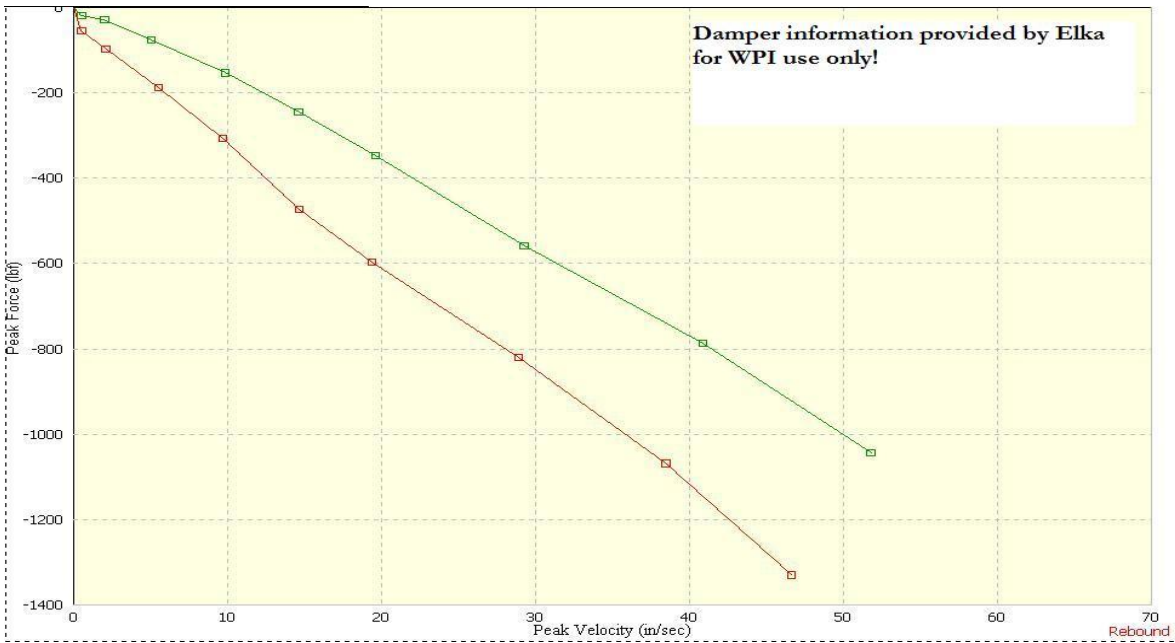


Figure 38: Front Rebound Damping

	Damper Force Linear Regression	
	Full Soft	Full Stiff
Compression	$7.95v - 36.5$	$10.95v + 152.5$
Rear Rebound	$-26.3v + 118$	$-37v + 100$
Front Rebound	$-21v + 55$	$-25.4v - 80$

Table 4: Damper Linear Regression

8.7 Appendix G: Front Suspension Design Results

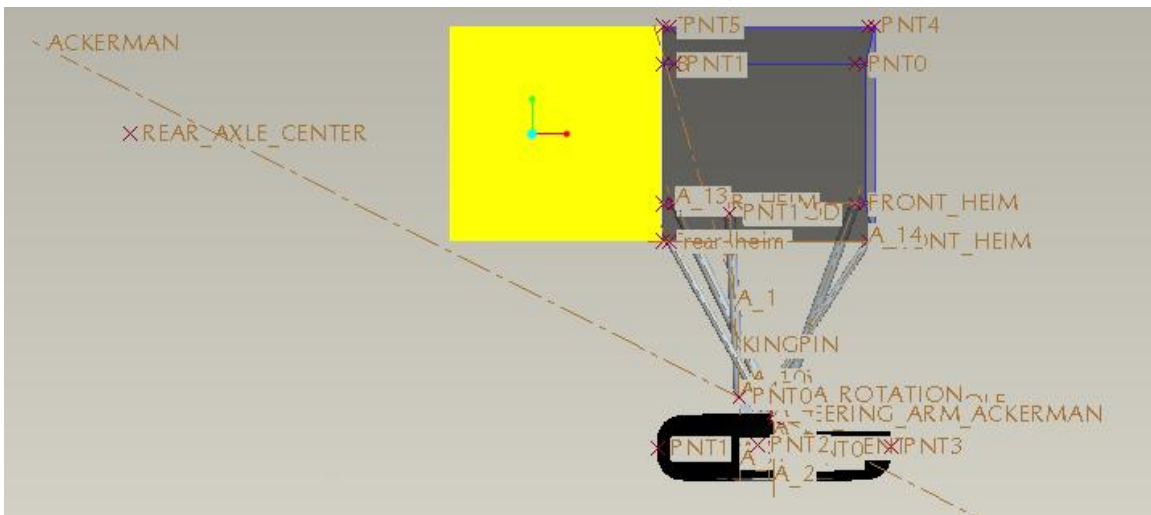


Figure 39: Steering Arm Angle Illustrating Ackerman Design

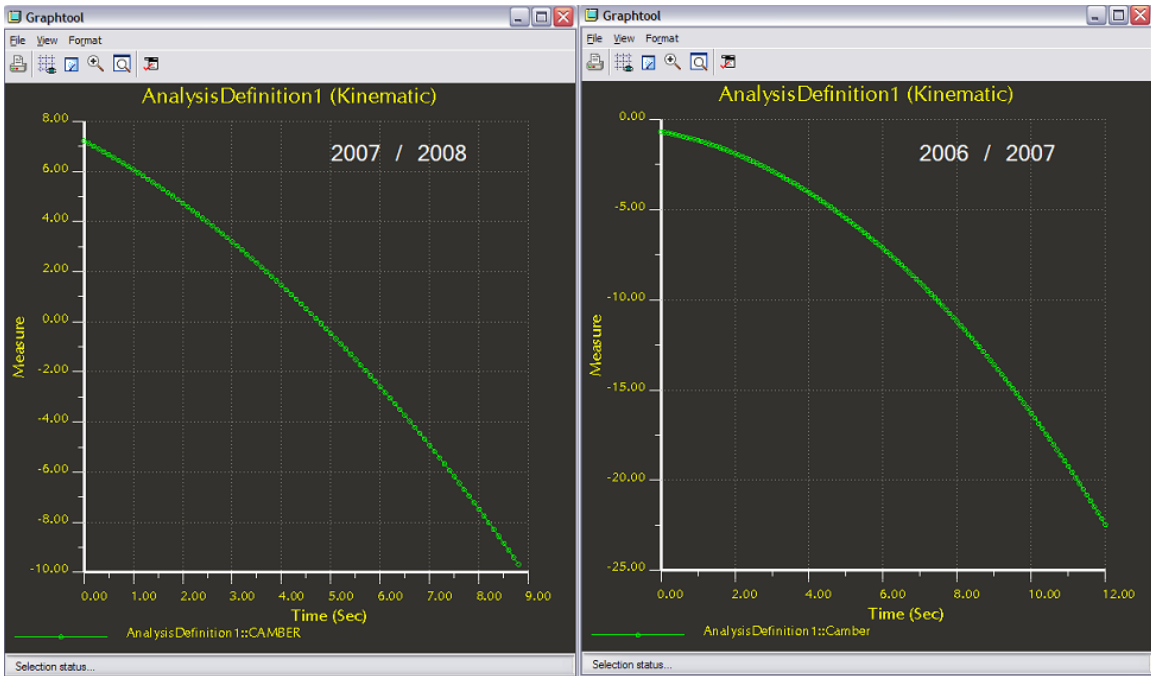


Figure 40: Comparison of Camber Curves

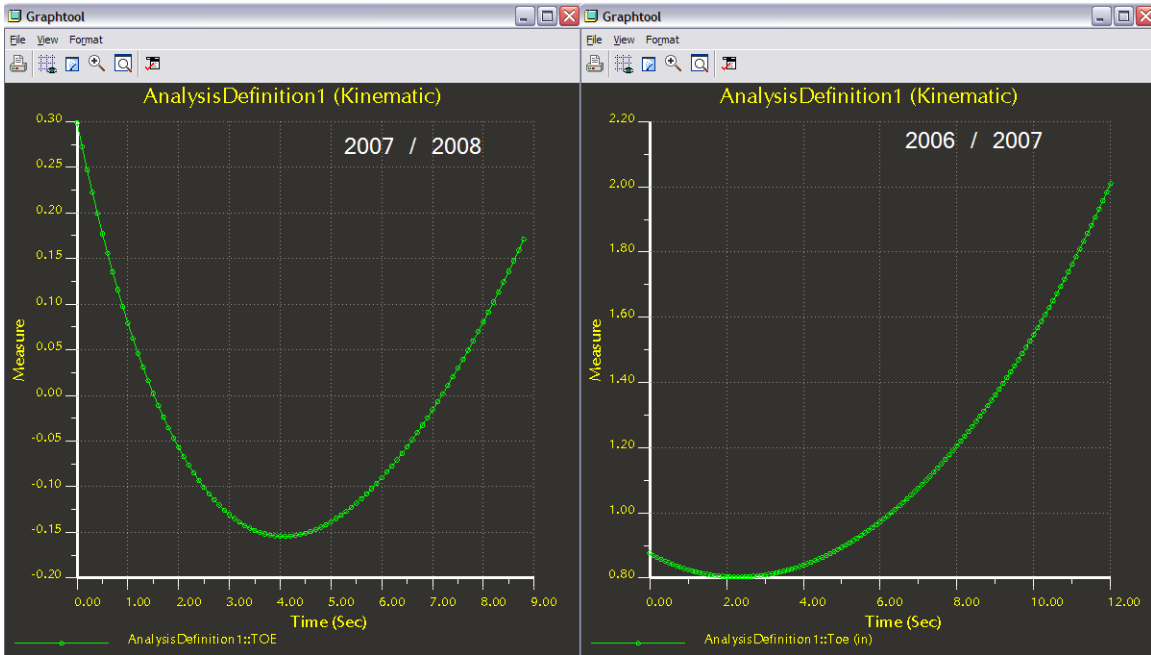


Figure 41: Comparison of Toe Change Across Twelve Inches of Travel

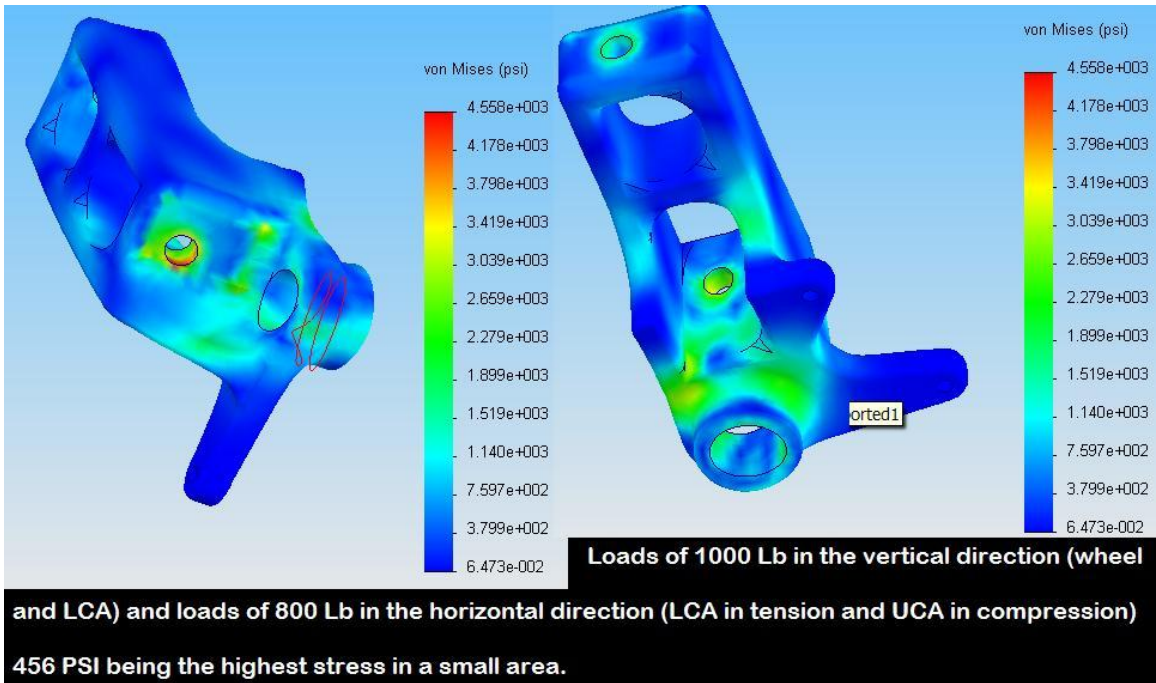


Figure 42: Knuckle Design FEA

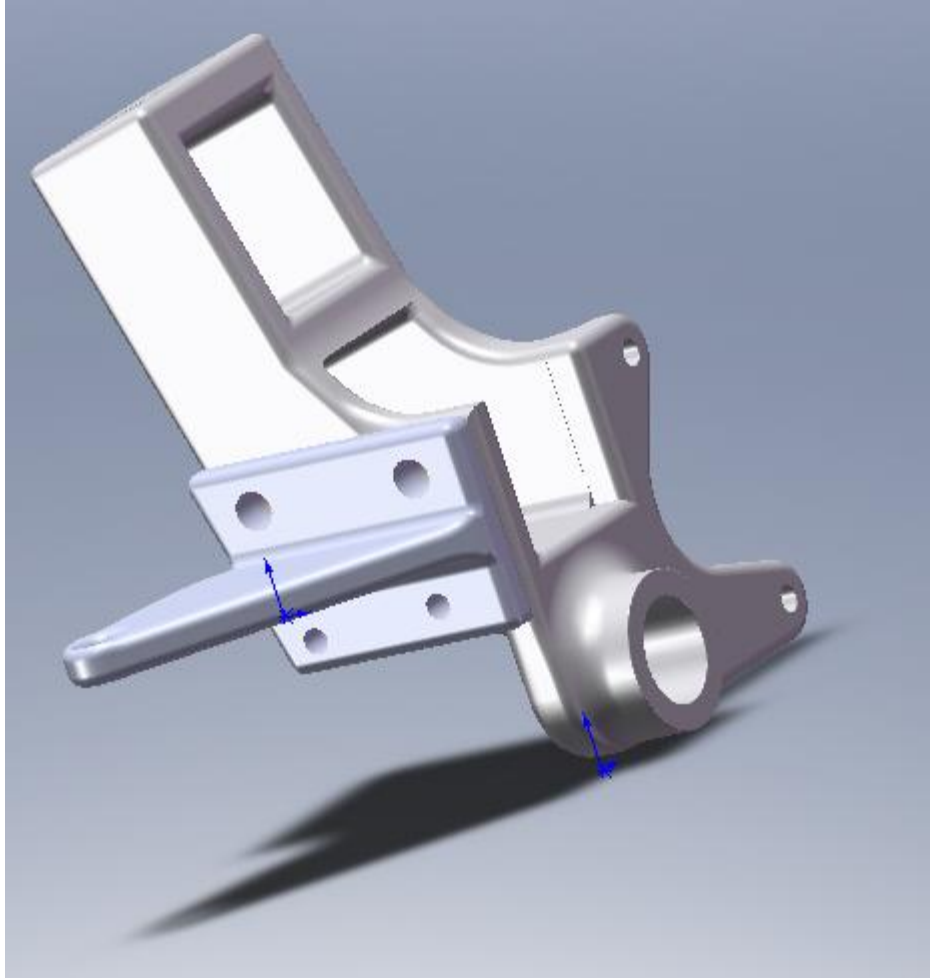


Figure 43: Final Knuckle Design with Detachable Steering Arm

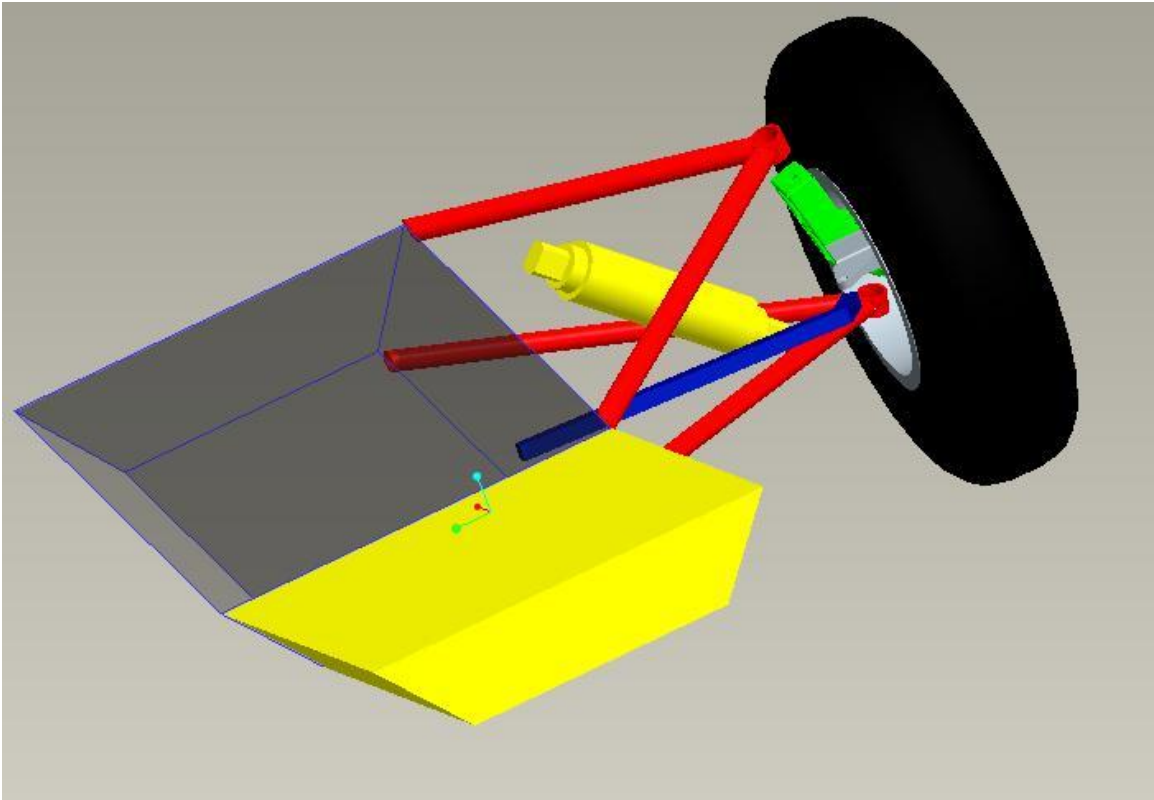


Figure 44: Front Suspension Overall Design